Assessing raindrop evolution over northern Western Ghat from stable isotope signature of rain and vapour

Sheena Sunil Nimya [1,2], Sundara Pandian Rajaveni[1], Saikat Sengupta[1*], Sourendra Kumar Bhattacharya[3], Nandhini Ananthvel[1]

[1]Center for Climate Change Research, Indian Institute of Tropical Meteorology, Ministry of Earth Sciences, Pune-411008, India

[2]Department of Earth, Atmospheric and Planetary Sciences, Purdue University, West Lafayette, IN, USA

[3] Institute of Earth Sciences, Academia Sinica, Taipei 11529, Taiwan

*Correspondence: Saikat Sengupta (saikat@tropmet.res.in)

Abstract

Rain and vapour isotopes were analysed in samples collected simultaneously from Pune, India, during the 2019 summer monsoon. The heavy isotopes of both oxygen and hydrogen ($\delta^{18}O$ and δD) were significantly depleted in four events when the Outgoing Longwave Radiation showed a strong negative anomaly, suggestive of large-scale convection. The $\delta^{18}O$ of the rain samples are negatively correlated with d-excess, indicative of modification of raindrops by evaporation. Analysis of the isotope data indicates isotope exchange between rain and ambient vapour and significant raindrop evaporation in the sub-cloud layer. The data plotted in terms of $\Delta\delta-\Delta d$, where Δ indicates the difference between rain-equilibrated vapour and the surface vapour, show an equal number of points lying in the 3rd and 4th quadrants, suggesting an equal share of two effects: equilibrium exchange with ambient vapour and drop evaporation.

We used a one-dimensional Below Cloud Interaction Model to quantify sub-cloud processes affecting raindrop evolution. A Rayleigh ascent assumption in BCIM overestimates rain isotope values, although model and observed values are well correlated. Using radiosonde-based temperature and humidity profiles and constructing vapour isotope profiles from a combination of satellite (Tropospheric Emission Spectrometer) data and a global circulation model (LMDZ) output, simulations improve and good agreement of the model with observed values is obtained. Sensitivity studies reveal that model outputs are strongly influenced by vapour isotope profiles, and moderately by drop size, temperature and relative humidity. Raindrop evaporation estimated from mass change in the model shows that, on average, 23 % of the drop mass evaporated in this region.

1. Introduction

The Intergovernmental Panel on Climate Change (IPCC) has emphasized the importance of recycled moisture in the atmosphere (IPCC, 2014). Moisture recycling includes processes by which a fraction of the precipitated water returns to the atmosphere and cause further precipitation over the same area (Gray, 2012). These processes are soil evaporation, transpiration from plants, intercepted or condensed water on leaves, and evaporation from falling raindrops (Brubaker et al., 1993; Trenberth, 1999). The moisture recycling increases with ambient temperature but decreases with increasing humidity (Pranindita et al., 2022; Zaitchik et al., 2006; Zhang et al., 2021). It has been seen (Kumar et al., 2021; Pathak et al., 2014) that a high precipitation recycling ratio (~15%) operates over India during the Indian Summer Monsoon (ISM; June-September). Among the recycled moisture sources, raindrop evaporation is difficult to estimate because (1) the parameters needed for estimating rain evaporation are not accurately available from satellite sources, and (2) station-based meteorological observations using Micro rain radars are limited (Dai et al., 2019; Li and Srivastava, 2001; Xie et al., 2016).

Stable isotopologues ($^{1}H_2{}^{18}O$, $^{1}H^{2}H^{16}O$, $^{1}H_2{}^{16}O$) of liquid precipitation samples can be used to assess the magnitude of raindrop evaporation (Crawford et al., 2017; Rahul et al., 2016; Salamalikis et al., 2016; Wang et al., 2021; Xiao et al., 2021). Falling raindrops exchange isotopes with the ambient vapour; this happens throughout the fall but occurs mostly in the unsaturated sub-cloud layer. The magnitude of this exchange, which alters the rain isotope ratios, can, in principle, be used to quantify the extent of raindrop evaporation. Using satellite-based observations of vapour isotopologues ($^{1}H^{2}H^{16}O$ and $^{1}H_2{}^{16}O$) and an isotope mass balance model, Worden et al. (2007) estimated that in the tropics, during the October to March interval, nearly 20 % of the mass of raindrops evaporates. However, they noted that the satellite data has limited temporal and spatial coverage. Therefore, estimating drop evaporation on a daily to monthly scale is difficult. Raindrop evaporation has also been estimated from ground-based rain isotope observations and a set of empirical equations (Froehlich et al., 2008; Li et al., 2021; Wang et al., 2016; Zhu et al., 2021). However, it remains a challenge to account for all cloud microphysical processes and their associated isotopic fractionations. Normally, these processes are considered for simulating rain isotope values in various General Circulation Models (GCM; Risi et al., 2019; Yoshimura et al., 2008; Stewart, 1975). However, recent studies have shown that most of these GCMs over or underestimate raindrop evaporation in tropical India (Nimya et al., 2022; Sengupta et al., 2023). This is possibly due to the coarseness of grid sizes used in these GCMs, which are inadequate to capture the region-specific complexities of processes controlling the evaporation. This necessitates controlled isotope observations and region-specific models for a reasonable estimation of this parameter (Aemisegger et al., 2015).

Various approaches have been followed to estimate raindrop evaporation using paired observations of rain and vapour isotopes. For example, a bin resolved microphysical model was used to quantify drop evaporation during the Atlantic Tradewind Ocean–Atmosphere Mesoscale Interaction Campaign (ATOMIC; Sarkar et al., 2023). Graf et al. (2019), based on surface rain and vapour isotope observations in Zurich, Switzerland, provided a rationale to evaluate various processes controlling the isotope values. They developed a simple one-dimensional model (Below Cloud Interaction Model, BCIM) which considers essential cloud microphysical processes during raindrop formation (vapour deposition, riming, etc.) as well as evaporative exchange processes within and below the cloud. That model determines the isotopic evolution of an ice/liquid

drop released from a desired altitude and undergoing exchange processes enroute its fall to the ground. However, being a one-dimensional vertical model, it does not consider any moisture advection, updraft and downdraft. Nevertheless, it is worthwhile exploring the efficacy of that model in a semi-tropical region like Pune during the ISM when advected moisture fluxes play an important role (Levine and Turner, 2012).

In the Western Ghat (WG) region, shallow convective clouds predominate (80 % of clouds occur below 4 km and 45 % below 2.5 km altitude) during the ISM (Konwar et al., 2014). Faster evaporation of smaller raindrops associated with intense rainfalls from these clouds provides significant positive energy feedback to form mesoscale convection (Konwar et al., 2014; Tao et al., 2012). A study of drop size distributions showed that raindrop evaporation prevails in the warm rain process occurring in this region (Murali Krishna et al., 2021). The current study investigates the applicability of the BCIM in a tropical Indian region using paired observations of rain and vapour isotopes for a summer monsoon season.

2. Experimental Methodology

2.1 Study area

Rainwater and vapour samples were collected from the ground level at the Indian Institute of Tropical Meteorology (18.53° N, 73.85° E), Pune during the summer monsoon of 2019. This region receives >90 % rainfall during the ISM and is situated at the lee (rain shadow) side of the Mountain (Fig. 1). Rainfall in Western India occurs from mid-tropospheric low-pressure systems in several episodes, each of which usually lasts for 2–3 days. These systems are locked in place during these periods and fed by moisture derived from the Arabian Sea (Wang et al., 2006; Rao, 1976). The geographic location of the region, its altitude, rainfall variation across the WG mountains, and the topographic profile across Pune are shown in Fig. 1. There is a sharp variation of rainfall across the mountain from the coastal zone (30 mm day^{-1}) to the lee side (12 mm day^{-1}) which is a characteristic of orography-induced rainfall (Fig. 1). The surface air temperature in Pune varies from 20° C to 30° C during the ISM (Pattanaik et al., 2019).

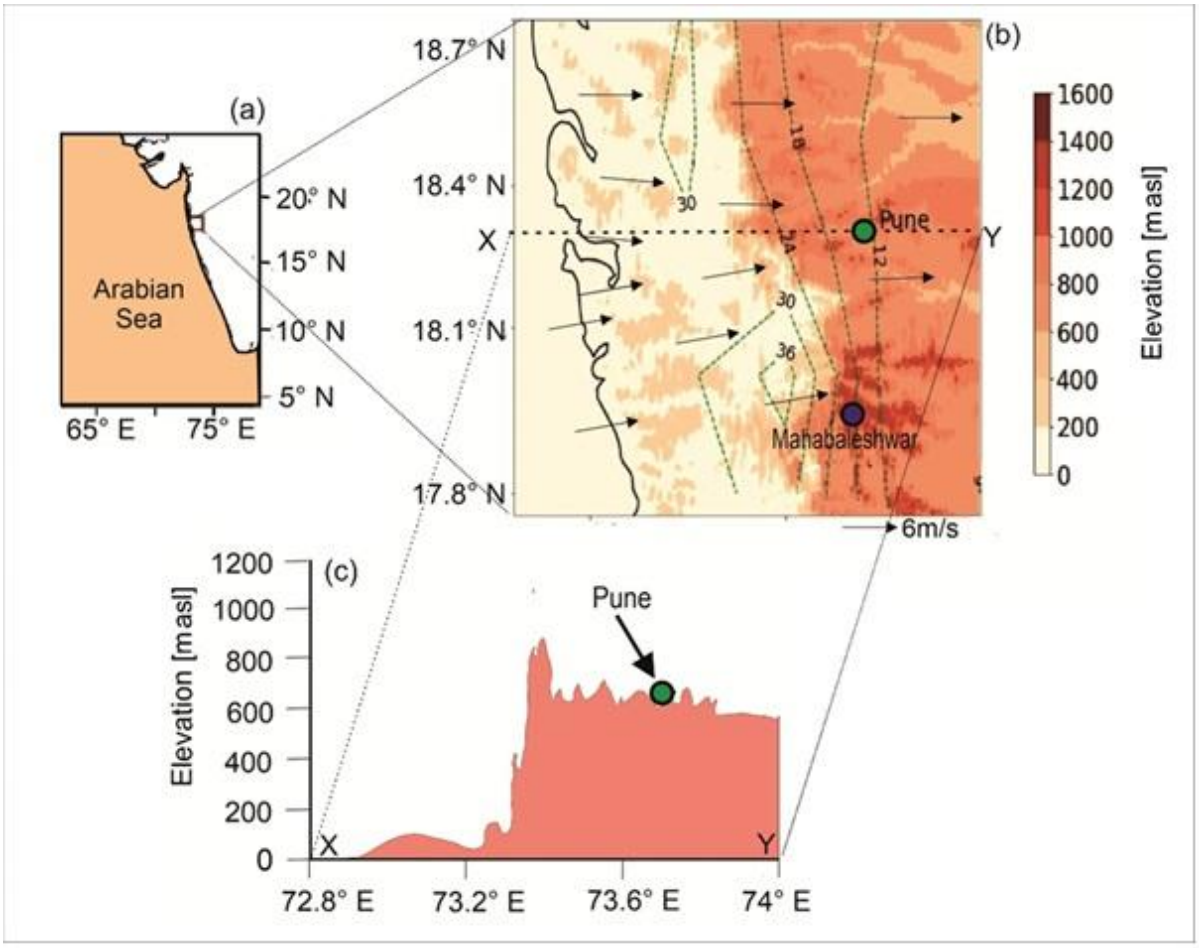

Figure 1. (a) The location of the study area in India. **(b)** Topographic map of the northern Western Ghat, India (prepared based on the GTOPO30 digital elevation model). The rainfall contours (long-term (1901-2017) mean June-September rainfall in mm/day) were constructed using gridded (0.25°x0.25°) rainfall data (1901-2020) from the India Meteorological Department (IMD). **(c)** A topographic profile along the latitude 18.53° N through Pune (Green circle at an altitude of 560 m) shows its position.

2.2 Sample Collection, Isotope Measurements

The onset and withdrawal dates of ISM (based on wind direction, specific humidity, and outgoing long wave radiation, OLR; IMD, 2019) at Pune in 2019 were 22 June 2019 and 4 October 2019, respectively. Liquid water samples were collected during rains using samplers made following the guidelines of the International Atomic Energy Agency (see Supplementary Information Fig. S1-1). For vapour samples, an in-house fabricated glass condenser was used (see Fig. S2-1). Most of the vapour samples were collected during the rainy days (avoiding direct raindrop entry), but some were also collected during the non-rainy period. The collection efficiency was estimated from the amount collected against the amount expected (see Table S2-1). Due to logistical problems, vapour samples could not be collected before mid-July. A total of 50 vapour samples were collected and 29 of them coincided with the rain sampling days.

The samples (rain water and condensed vapour) were measured using a Liquid Water Isotope Analyser (Model Number TIWA-45-EP, Los Gatos Research). This instrument measures liquid samples using Off-Axis integrated cavity output spectroscopy (OA-ICOS) with a routine precision of 0.1 ‰ and 1 ‰ for $\delta^{18}O$ and δD

(relative to VSMOW) respectively (Rajaveni et al., 2024; see also Supplementary Information SI-3). The d-excess values defined as: d-excess = $\delta D - 8 * \delta^{18}O$ (Dansgaard, 2012) have a precision of 1 ‰. The daily rain isotope data are weighted by the amount of rainfall on that day.

2.3 Satellite and ground-based meteorological data

The rainfall data are obtained from the Pune observatories of the IMD, available at the National Data Centre (www.imdpune.gov.in/ndc_new/ndc_index.html). Apart from rainfall, daily average temperature and relative humidity data for the Pune observatory were also obtained. The daily gridded data (zonal and meridional wind, specific humidity, air temperature, and cloud liquid water content) from the European Centre for Medium-Range Weather Forecasts Reanalysis (ERA5) dataset with a resolution of 0.25° × 0.25° (Hersbach et al., 2020) and the Interpolated Outgoing Longwave Radiation (OLR) data (2.5° × 2.5°) from NOAA (https://psl.noaa.gov/data/gridded/data.olrcdr.interp.html) are used in this study. The upper-air radiosonde measurements (relative humidity, temperature) carried out over Pune were obtained from the University of Wyoming repository (http://weather.uwyo.edu/upperair/sounding.html). The vertical variation (every 50 mb interval) of the two parameters was available for two times: at 00 UTC and 12 UTC, and for each parameter, the two profiles are averaged to make a representative daily profile. The typical uncertainty of temperature and relative humidity is 0.3° C (Sapucci et al, 2005; Jensen et al., 2016) and 8 % (Xu et al., 2023), respectively. Tropospheric Emission Spectrometer (TES) Level 2 (Nadir-Lite-Version 6) retrievals of HDO and H_2O profiles for the available period (2005–2007) are used to construct mean vapour δD profiles. The details of quality control criteria and biases associated with TES observations are discussed by Herman et al. (2014) and Worden et al. (2011). Grid point observations of δD by TES have a precision of ~ 10–15 ‰, which reduces to 1–2 ‰ when the data are averaged over a larger region (Lee et al., 2011; Pradhan et al., 2019).

To decipher the moisture sources for vapour/rain at and around our study area, 48-hour air mass back trajectory analysis was carried out at 850 mb pressure level using the NOAA Hybrid Single-Particle Lagrangian Integrated Trajectory (HYSPLIT) model (Draxler and Hess, 1997). The model tracks the movement of air parcels backward from a given location for a desired period (see SI-4).

2.4 The input parameters for BCIM

Various parameterisation schemes used in the BCIM have been discussed by Graf et al. A brief description of this model, as applicable for the shallow cloud processes over Pune, is provided here. The model comprises a single vertical column that extends from the ground level to the point at which a single hydrometeor is introduced. Within this column, the hydrometeor descends under the influence of gravity, undergoes growth or evaporation (depending upon the ambient humidity and temperature), changes its isotopic composition through equilibrium and kinetic isotope exchange with surrounding vapour, and finally reaches the surface as raindrop. The final isotopic composition of the hydrometeor is estimated following four steps of calculations: (1) setting up the initial condition involving the drop introduction height and its size, (2) estimation of the initial isotopic composition of the hydrometeor, (3) microphysics of falling hydrometeor, and (4) tracking the changes in isotopic composition along the descent. For these calculations, the model requires temperature, humidity and vapour isotope altitude profiles for a given day as input parameters. The drop is assumed to form in equilibrium

(at relative humidity, RH=100 %). The input parameters for the vapour can be introduced into the BCIM in two different ways: (1) the profiles can be calculated based on assumption of idealised (moist) adiabatic ascent of an air parcel from the surface to the top of the column following a Rayleigh model; RH, T and isotope values at various pressure levels are then estimated from the Rayleigh distillation equations starting from the measured surface values or (2) the pressure level specific values of RH and T from radiosondes and isotope values from satellite data and/or any model.

Since our aim is to understand the isotopic modification and mass loss suffered by the drops on the way down, we introduce here two parameters δ and Δd expressing the deviation of the final rain composition at the ground from the ambient surface vapour. For this, we use the difference between the isotopic composition of vapour in equilibrium with the rain samples and the ambient surface vapour and define: $\Delta\delta = \delta D$ (rain eq. vapour) - δD (surface vapour) and similarly for d-excess, Δd = d-excess (rain eq. vapour) - d-excess (surface vapour).

2.4.1 Drop size assignment

The model also requires the input diameter of the initial hydrometeor. Unfortunately, no disdrometer or Micro Rain Radar observations are available for Pune during 2019. We, therefore, adopted an empirical procedure, known as the Marshall-Palmer (M-P distribution) relationship (Marshall and Palmer, 1948), to estimate the mean drop size at the ground. First, we estimated the hourly mean drop size of the raindrops at the ground level from the hourly rain rate data, available from the IMD observatory at Shivajinagar, Pune, located about 4 km away from the sampling location. Next, we calculated the 24-hour mean drop size by taking a weighted average of the size using rain rates as the weights. The calculated drop sizes at the ground vary from 0.61 to 1.80 mm for various days. The drop diameter at the ground is next provided as an input and the initial size at the drop introduction height (about 2.0 km above ground) is estimated iteratively in BCIM using the microphysics part of the model, using the temperature and RH profiles. This procedure was adopted for each day. The accuracy of the drop size based on the M-P distribution and the rain rate is limited, but this was the only imperative since no drop size (disdrometer) measurements were available. Our choice was guided by earlier modelling and observational studies where the M-P distribution was used (Graf et al., 2019; Sarkar et al., 2023; Morrison et al., 2020; Ryu et al., 2025; Jiang et al., 2024).

2.4.2 Drop formation height assignment

The formation height of the drop should be fixed by considering the most probable altitude range where the majority of the drops exist on any given day. This was not known a priori and was inferred from the cloud liquid water content analysis. An earlier study by Kumar et al. (2014) showed that a peak of Cloud Liquid Water Content (CLWC) is often present at about 850 mb during the monsoon season over western India. In the present case, the CLWC data for 29 days of the study period obtained from the ERA5 dataset show a peak at 830±70 mb, i.e., about 1650 m above msl (See Table S5-1 and Fig. S5-1). Here, we consider the CLWC peak of a given day as the drop introduction height for that day.

In the present study, we consider the cloud base height as the Lifting Condensation Level (LCL) where RH is 100%. The RH and T profiles from the radiosonde data at various heights (with extrapolated ground level values; see SI-8b) are used to estimate the LCL using the Skew T-Log P diagram for all 29 sampling days. The

LCL varies from 820 to 900 mb, and the average height is 890 ± 20 mb (about 1050 m; see Table S5-1). We notice that the LCL is always below (about 600 m on average) the corresponding day's CLWC peak, as it should be, and therefore, the drop falls through a zone of 100% RH till it emerges below the cloud base or LCL (see SI-5).

2.4.3 Isotopic composition of the ambient vapour and hydrometeor

The isotopic composition of the introduced hydrometeor is estimated by assuming formation in equilibrium from the vapour at this altitude at the ambient temperature. Subsequently, these drops grow or diminish as they fall. The isotopic composition of the falling hydrometeor at lower altitudes is then calculated from the composition of the surrounding vapour by using isotope mass balance and diffusive transport involving appropriate fractionation factors (Graf et al., 2019).

The mass and temperature of the hydrometeor are calculated along its fall trajectory using the microphysics of the falling hydrometeor. The terminal velocities are estimated using Foote and du Toit (1969). To calculate the change in mass and temperature between two pressure levels, the temperature, pressure, and humidity values are interpolated between these two levels. These changes are estimated as per Pruppacher and Klett (2010). It is important to mention here that many processes considered in BCIM do not occur for the shallow convective clouds in Pune (Utsav et al., 2017). Therefore, the BCIM inputs are taken accordingly in the present study.

3 Results

We present the results of the current study in two sections: (1) Results of isotope analysis and (2) Results of BCIM simulations. The first section presents the measured isotope ratios in the context of meteorological parameters, whereas the BCIM simulations are compared with the measured values in the second section.

3.1 Results of isotope analysis

Measured rain and vapour isotope ratios ($\delta^{18}O$ and d-excess) on a daily scale are plotted in Fig. 2a and 2b. The general pattern of variations in vapour and rain $\delta^{18}O$ values is similar; both decrease significantly and consistently after mid-August. The vapour δ-values are lower than the rain. In contrast, the d-excess values of vapour are always much higher. The $\delta^{18}O$ and d-excess values of rainwater range from −10.8 ‰ to 1.5 ‰ and −2 ‰ to 12 ‰, respectively, while those of the vapour range from −19 ‰ to −9 ‰ and 10 ‰ to 30 ‰, respectively. The mean and 1σ standard deviation of $\delta^{18}O$ and d-excess values of rainwater are −1.3±2.6 ‰ and 3.9±2.7 ‰, while those of the vapour are -12.5±2.5 ‰ and 18.3 ± 5.2 ‰, respectively. The $\delta^{18}O$ (Fig. 2a) and d-excess (Fig. 2b) time series show four interesting features: (1) For the four date ranges: 27-29 July, 24-27 July, 4-8 September, and 19-27 September, significant and consistent decrease in isotope values are observed in both rain and vapour phases (marked 1, 2, 3, 4 in Fig. 2a; no vapour data available for date range 1), (2) On 19 September, the vapour shows sudden decrease (marked A in Fig. 2a), (3) there is a gradual decrease in vapour $\delta^{18}O$ values and an increase in d-excess values with the progress of the monsoon, especially more in the later part, and (4) rain d-excess values remain constant with time but $\delta^{18}O$ of both rain and vapour start decreasing beginning from early September onwards.

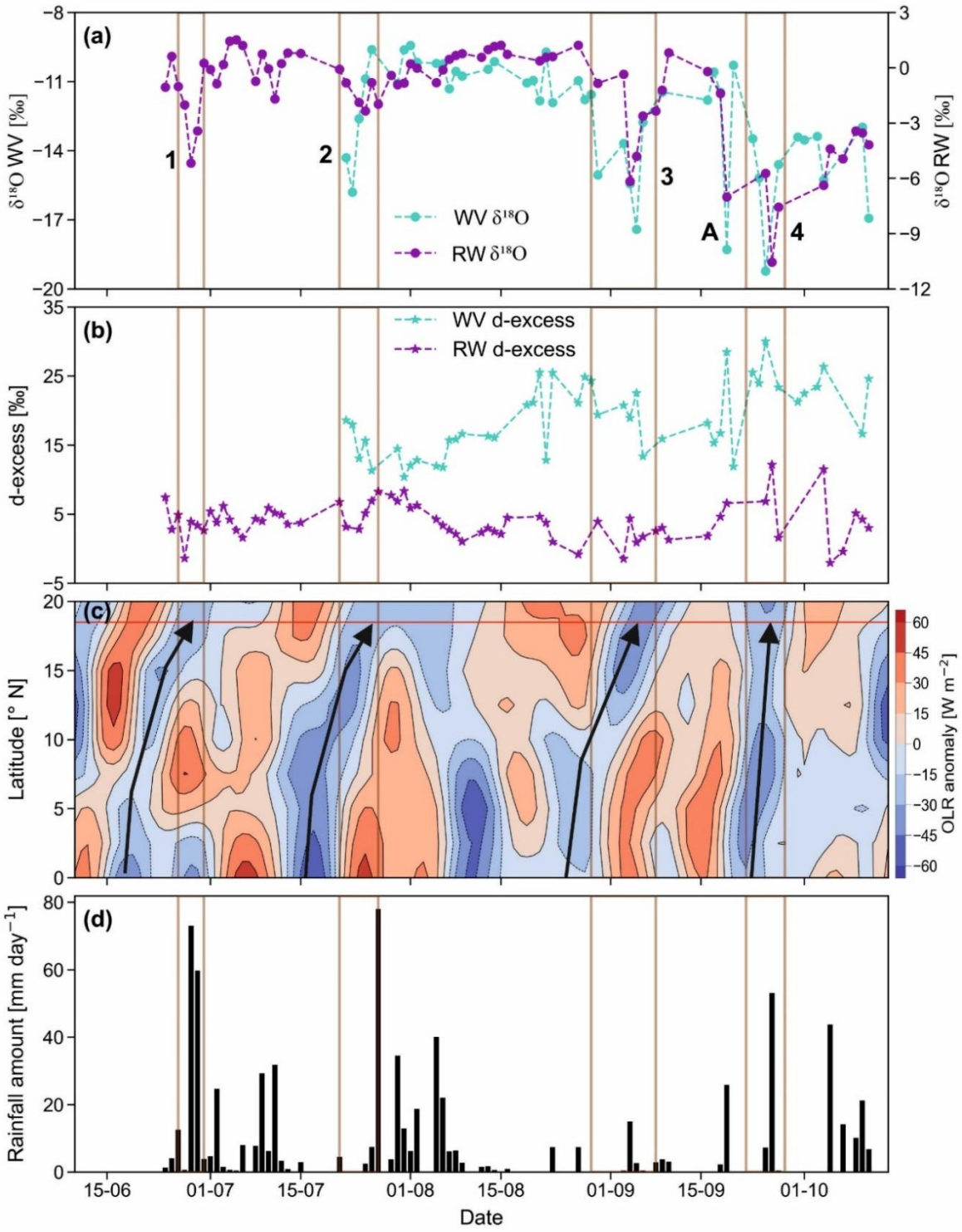

Figure 2. The time series of $\delta^{18}O$ **(a)** and d excess values, **(b)** of the rainwater (RW) and water vapour (WV), **(c)** OLR anomaly (W m^{-2}), and **(d)** daily rainfall (mm over 24 h; d) in Pune. The four vertical boxes (numbered 1, 2, 3, and 4) denote synchronous low OLR values and low isotope values (i.e., less than their respective μ-0.5σ values). These periods are defined as low isotope events. A indicates one isolated low isotope value without low OLR association. Thick arrows show how convective cloud bands (indicated by low OLR anomaly) traverse to the sampling region over Pune from South-west. Note highly depleted values on 19, 25 and 27 September.

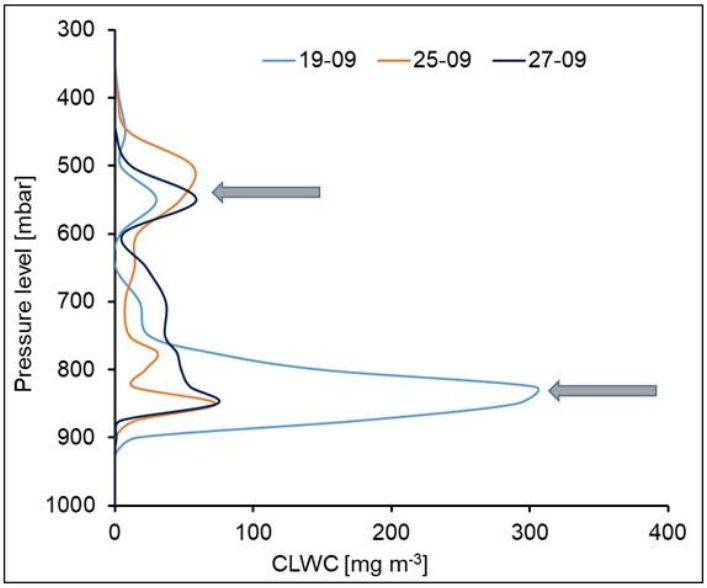

Figure 3. Presence of second CLWC peaks at higher altitudes (about 550 mb) on 19, 25 and 27 September 2019 (beside the first major peaks at lower altitudes) when highly depleted rain $\delta^{18}O$ values were observed in association with negative OLR anomaly (see Fig. 2). The altitudes of the two sets of peaks are shown by two arrows.

Isotopic depletions in rain and vapour samples in the tropics are often associated with deep convection (Lekshmy et al., 2014; Risi et al., 2008; Sengupta et al., 2020), whose signature is possibly present in the present data in the form of depleted-isotope events. We define depleted-isotope events as those where isotope ratios of a group of samples fall below the overall mean (μ)-0.5 standard deviation (σ) (Sengupta et al., 2020). To examine the extent to which the depleted (more negative) isotope events are related to large convective events, a latitude-time Hovmoeller plot of daily OLR anomaly (averaged over the longitude 70° E -75° E) is displayed in Fig. 2c. The OLR values are often used as a proxy for convection in tropical and subtropical regions. Since the cloud top temperatures are an indicator of cloud height (colder is higher), a negative OLR anomaly means colder cloud top temperatures or higher cloud thickness. This, in turn, implies extensive coverage by deep cloud systems, characteristic of mesoscale convection and rain. A time synchronous association of low OLR and depleted-isotope events thus indicate mesoscale convection affecting isotope values. Fig. 2c indicates four such isotope-depleting mesoscale events (marked as 1, 2, 3 and 4 in Fig.2a). In addition, we also see one depleted-isotope event without such association (marked as A in Fig. 2a). We also note that there were significantly high second CLWC peaks on the three days, 19, 25 and 27 September, at much higher levels (about 550 mbar or about 5.5 km altitude) shown in Fig. 3 (corresponding to the event number 4 mentioned above).

We note from Fig. 2d that major rainfall occurred during the months of July and August; the relative humidity at the surface during the whole monsoon season varied from 71 % to 97 %, and the surface temperature varied from 25° C to 30° C (see Fig. S10-1). It is evident from Fig.2d that deep convection is associated with high rainfall for the three events 1, 2, and 4. A recent study, based on a year-long continuous measurement of atmospheric vapour in Sri Lanka (a nearby tropical country under similar monsoon system) also

found such isotopic depletion during high rainfall events (Wu et al., 2025).

Fig. 4a shows the local meteoric water line (LMWL) using rainwater samples and the local water vapour line (LWVL) using vapour samples from this study. The LMWL equation is $\delta D_r = (7.3\pm0.1)\ \delta^{18}O + (3.0\pm0.3)$ and the LWVL, $\delta Dv = (6.4\pm0.2)\ \delta^{18}O - (1.9\pm3.0)$, subscripts r and v denote rain and vapour. The slope and intercept of the LMWL values are lower than those of the Global Meteoric Water Line (GMWL), which are 8.0 and 10.0, respectively (Dansgaard, 2012; Gat, 1996). This difference, though small, suggests some amount of below-cloud evaporation of the rains. At Roorkee, a high-latitude Indian Station, Saranya et al. (2018) found an LMWL with a lower slope (5.4) but a higher intercept (27). They attributed these changes to the contribution of evaporation from water bodies nearby and moisture recycling during the monsoon. Rahul et al. (2016) got a similar slope (7.4) but a lower intercept (1.5) in Bangalore (southern central India, at a high altitude of ~1 km). The lower slopes of meteoric water lines provide a signature of evaporation processes associated with kinetic fractionations occurring during rain.

The d-excess values of rain samples suffering evaporation generally bear a negative relationship with $\delta^{18}O$ values (Bonne et al., 2014; Munksgaard et al., 2020). This is also seen in our study (Fig. 4b**)** where rain d-excess decreases with an increase in $\delta^{18}O$ values. In addition, the vapour d-excess values also show a statistically significant negative correlation with $\delta^{18}O$ values (Fig. 4b; $R^2 = 0.61$; $p = 0.001$), probably indicating contribution of vapour derived from rain evaporation (Kurita, 2013; Risi et al., 2021). Correlation studies can be indicative, but the causative factors behind the above variations can be explored only with the help of a process-based model like BCIM.

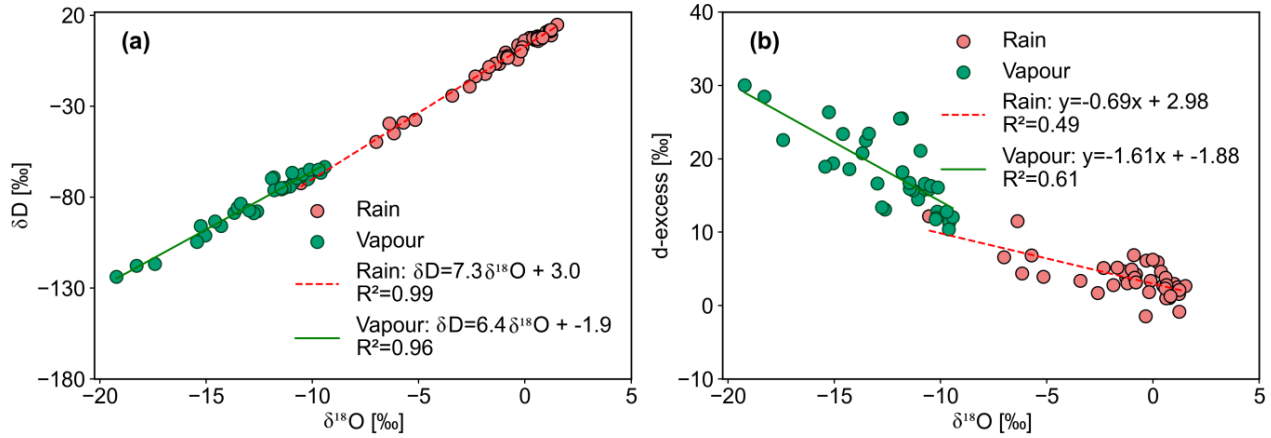

Figure 4. A cross-plot of **(a)** δD and $\delta^{18}O$ of rain and vapour; **(b)** a cross-plot of d-excess and $\delta^{18}O$ of rain and vapour showing anti-correlation. Mean regression lines and correlation coefficients are shown inside the plots.

3.2 Results of BCIM simulations

As discussed in section 2.4, simulation runs of BCIM were carried out under three assumptions about the vertical profiles of RH, T and vapour isotopes. The results are shown as Run-1, Run-2 and Run-3, which were designed to make progressive improvement in reproducing the measured rain isotope data.

3.2.1 Run-1: Rayleigh ascent

The sources of input profiles of ambient temperature (T), relative humidity (RH), vapour δDv, and vapour d-excess (dv) required for three BCIM runs are given in Table 1. In Rayleigh simulations (designated as Run-1), the profiles were calculated using the equations for moist-adiabatic ascent of air parcels (see Appendix A1 of Graf et al.,2019) starting at the surface with values of temperature (T_0), relative humidity (h_0), δDv (δv,0) and dv (dv,0) of each sampling day as inputs. The surface values of δD and d-excess of vapour (denoted by the symbol d) were taken from our vapour measurements along with the daily average temperature and humidity values obtained from the surface observations of IMD (Section 2.3). A dry adiabatic ascent formula is used in the initial phase up to the cloud base (LCL). Above the cloud base, a moist-adiabatic lapse rate is used. The dry and moist lapse rates are calculated using equations based on the gravitational constant, specific heat of dry air, mass mixing ratio of vapour, latent heat of evaporation, specific gas constant of dry air, temperature, ratio of specific gas constants of dry air and water vapour, specific humidity and saturation vapour pressure. The input profiles of RH, T, δDv, and d-excess for all 29 sampling days are given in Supplementary Information (Fig. S8b-1 and Fig. S8b-2).

Table 1. Input parameters for various BCIM runs

Sl. No	BCIM input	Parameters for Run-1	Parameters for Run-2	Parameters for Run-3
1	Drop size	Marshal-Palmer equation using hourly rainfall data obtained from IMD	Same as Run-1	Same as Run-1
2	RH profile	Rayleigh ascent ~15 % increase per km and 100% above CBH to drop introduction height	Radiosonde values normalized to surface observation and changed to 100% above CBH to drop introduction height	Same as Run-2
3	Temperature profile	Rayleigh ascent Lapse rate ~ 5.6°C km^{-1}	Radiosonde normalized to ground value	Same as Run-2
4	δD_{vap} profile	Rayleigh ascent ~7 ‰ decrease per km	TES normalized to measured surface value	δD values reduced slightly (within ±4‰) keeping the shapes like Run-2
5	d-exc_{vap} profile	Rayleigh ascent ~0.1 ‰ increase per km	LMDZ δD and $\delta^{18}O$ values used to get d-exc_{vap} normalized to measured ground value	d-exc_{vap} decreased from Run-2 average of 17‰ to an average ~10‰
6	Rain drop formation height (CLWC peak)	ERA5 Cloud Liquid Water Content peak	Same as Run- 1	Same as Run- 1
7	Cloud Base Height (LCL)	LCL from radiosonde profiles using skew-T log P diagram	Same as Run-1	Same as Run-1

3.2.1.1 Run-1 results

Results of Run-1 simulations are compared with the observed values of rain δD (Fig. 5a), $\delta^{18}O$ (Fig. 5b), and d-excess (Fig.5c) values. We also construct Δδ−Δd cross plots for both observed and model values in Fig. 5d. Although observed and model isotope values (Fig. 5a and 5b) show strong correlation (R^2=0.86 and 0.79, respectively), the model values are mostly overestimated (the plotted points lie below the 1:1 line). The overestimations of isotopes (for $\delta^{18}O$ and δD) affect the d-excess values considerably more; the points lie far to the right, and no correlation exists between the observed and model d-excess values (Fig. 5c). This is because the d-excess parameter is more sensitive to departure from equilibration, which means that a small departure of delta values would magnify the discrepancy in case of d-excess. We also note that most of the model data points in the Δδ−Δd cross-plot do not agree with the observed data points and lie closer to the origin. However, many of the model points fall in the lower right quadrant, which is expected in the case of dominant raindrop evaporation. We also note that the Δδ and Δd values (Fig. 5d) show smaller variations compared to the observations. The Δδ of the model simulations varies from 0 ‰ to 5 ‰ and Δd from 0 ‰ to -5 ‰, while the observed values have variations of about 25 ‰ (higher by a factor of 5). These comparisons show that the Rayleigh ascent model with the prescribed inputs fails to reproduce the evolution of the rain isotopes in our region. We suspect that the vertical profiles of RH, T and vapour isotopes need to be modified to improve the simulations. Rayleigh ascent in Run-1 assumes that the source of vapour aloft is an unaltered rising air parcel with constant specific humidity. But we see from Fig. S5-2 and S8b-1 that this condition results in unusually low cloud base over Pune (i.e., the level where RH attains the value of 100%), which is not observed (Naik et al., 2003). In fact, the ERA5 data show that specific humidity decreases with height (Fig. S6-1). It is well known that a decrease in specific humidity is associated with a decrease in the vapour isotope ratios (Noone, 2012; Worden et al., 2007; see SI-6 for details). The simulation can possibly be improved if we use RH and T data from local radiosonde observations and try out altogether different isotope profiles having realistic vertical variations.

3.2.2 Run-2: RH and T from Radiosonde and isotope profiles from TES and LMDZ

3.2.2.1 RH and T from Radiosonde

For the study period, the average radiosonde observations were available (see section 2.3) at every 50 mb pressure interval (about 470 m), but the input for BCIM is required at every 1-meter interval. Therefore, a linear interpolation between every two consecutive pressure levels in logarithmic scale (Ingleby et al., 2016) was carried out to obtain RH and T values at meter levels. As the BCIM requires RH=100% for the formation of water droplets (considered to be at CLWC peak level), the RH values above the lifting condensation level (LCL) were considered as 100% disregarding the radiosonde data above the LCL (see section 2.4.2 and SI-8b).

3.2.2.2 Vertical profiles of vapour isotopes from TES data

To obtain the vertical profiles of vapour isotopes, we first tried out the isotope outputs of a General Circulation Model, namely, LMDZ. The output data for our sampling days over Pune was provided by Dr. Camille Risi (personal communication, 2023) using the LMDZ isotope-enabled general circulation model (GCM), known as LMDZ-iso (Risi et al., 2010), which is a version of the LMDZ atmospheric model adapted to simulate the natural variations of water isotopes in precipitation and vapour.

Initially, the LMDZ-derived values were also used in BCIM as inputs, but we found that a wide difference exists between the observed and model isotopic values (results not shown). We suspected that the LMDZ model did not generate the input vapour isotope profiles accurately. Possibility of such a limitation was noted by Risi et al. (2021), who observed that for high precipitation areas, the convective or mesoscale downdrafts bring depleted vapour from above into the sub-cloud layer.

Recognizing the large discrepancies arising out of using a GCM product (LMDZ) directly for both the isotopes, we tried out next the measured δDv profiles obtained from Tropospheric Emission Spectrometer (TES) observations pertaining to the Pune region. We should note here that the TES data were not available for 2019 and the available values must be modified for adapting to 2019 monsoon period. To account for the time discrepancy, the final profiles are constrained by using the measured daily-scale ground-level vapour isotope ratios as a boundary condition while maintaining the shapes of the TES δDv profiles. We should also mention here that apart from TES the vapour δD data, in principle, can be obtained from one other source, namely, Atmospheric Infrared Sounder (AIRS). However, isotope vertical profiles obtained from AIRS and used in the BCIM runs (after suitable modifications) produced rain isotopes that were widely different from the observed values. See Supplementary Information SI-7 and Fig. S7-1.

The derivation of vapour isotope profiles applicable for our sampling days in 2019 requires an adjustment, which would allow merging of lower-level data with the TES observations at upper layers. This assumes that the shapes of the TES average profiles were applicable as far as the vertical variation is concerned. The TES satellite provides δDv values of moisture at 17 pressure levels with a 5.3 km × 8.4 km footprint during the years 2005-2009 over a box covering the study region (16°-20° N; 72°-76° E). Using these data sets, we can derive an average TES profile and assume it to be representative of the shape of the mean monsoon profile Our station at Pune falls within this box, but there is an inherent assumption that the average over a ~45 km^2 area represents a small sampling location. The only justification is the use of a boundary constraint where the TES average profile is adjusted to match the measured ground vapour value at the sampling location. In addition, the back-trajectory analysis indicates that the moisture source is always from the Arabian Sea, where the vapour is carried inland by the streaming air mass (see Fig. S4-1). Interestingly, an average of 17 years of data of $\delta^{18}O$ of rain waters in Bombay (from 1961 to 1978) is -1.3‰ (Bhattacharya et al., 2003), close to the Pune average value of -1.1‰ from the present study. It shows that Pune being located 150 km upstream of Bombay receives moisture of similar composition as Bombay (possibly added by some evaporation component on the way). Therefore, our assumption of a large areal average representing a small location is not expected to be wrong, at least as far as the vertical variation is concerned.

3.2.2.3 The adjustment technique to derive the vapour isotope profiles

The δD and d-excess profiles for each date from the TES data were obtained by adjustment with the measured surface values. We analysed the available TES δD profiles (digital values) for the years 2005-2007 and adopted three profiles from the data sets which correspond to the Minimum, Mean and Maximum surface vapour δD values observed in the present study at the surface level. Each of these three profiles was fitted with polynomials and the coefficients of these polynomials were treated as functions of the surface values. Once we get these functions, we can obtain the vapour isotope profiles for any day by using that day's surface value. This exercise was necessary to translate the digital TES values into an analytical form, allowing for the easy

calculation of vapour isotope values at each height (at one meter resolution required for the BCIM inputs) from the uppermost drop introduction point to the ground level, resulting in a smooth shaped profile.

A similar exercise was conducted to obtain the daily d-excess profile from the LMDZ GCM output for Pune in 2019 and normalising the profile to the measured vapour d-excess value. In brief, this was done by using the available δD and $\delta^{18}O$ profiles from LMDZ output for three cases (Mean, Max and Min surface values), fitting 4^{th}-order polynomials: $Ah^4+Bh^3+Ch^2+ Dh + E$, and then constructing the d-excess profiles for three cases with five coefficients. Five coefficients were used to get higher precision in fitting. Again, fitting was done for each of the polynomial coefficients (A, B, C, D and E) as a function of surface value and then used them to get the dex profile for each day. This procedure is discussed in detail in SI-8a. Fig S8b-1 and Fig S8b-2 in the Supplementary Information SI-8b show the input profiles (RH and T), and (δDv and d-excess) respectively, for the three runs, Run-1, Run-2 and Run-3.

The above exercise means that by using the observed ground vapour value as a boundary value, we obtain the desired profiles for δD and dex for each day from an analytical fitting of digital data from TES (adopted) and LMDZ. We used a multi-order polynomial to get the fitting as accurately as possible, especially for d-excess. Obviously, this method of estimating the vapour profile, constrained by surface vapour measurements, assumes that the vapour aloft is related to the surface value. This assumption may not be strictly correct. But it allows us to check if the BCIM, under the surface constraints, yield better rain isotope ratios at the ground compared to the Rayleigh model while being consistent with the TES measurements of vapour aloft.

3.2.2.4 Run-2 results

The above profiles were employed in BCIM to generate the daily-scale $\delta^{18}O$, δD and d-excess values of surface rains (Fig. 5e-5h). However, the results do not show much improvement compared to the Run-1 (Fig. 5e-5g) despite showing a larger variability in the Δδ–Δd plot (Fig. 5h); the Δδ values varied from -4.7 ‰ to 11 ‰ and Δd from -1.8 ‰ to -12.4 ‰. As in Run-1, all the model data points fell in the 3^{rd} quadrant of the Δδ–Δd cross plot (Fig. 5h and Fig. 5d). Both Run-1 and Run-2 simulations fail to yield a good match between the observed and model values (especially the d-excess). The rain δD values differ by about -8 ‰ to 20‰. The model d-excess values are higher (by 0 to 15‰). Interestingly, the model rain values of Run-1 and Run-2 are quite close (within ±2.5‰) despite RH and T and isotope profiles being very different. This suggests that the assumption of surface vapour value as the boundary constraint, as used in both these runs, is the main determinant for rain isotopes.

3.2.3 Run 3: Tuning of Vapour Isotope Profile

The mismatch in the case of Run-2, as discussed above, indicates that we still need to modify the input profiles to obtain a better match with the observed values. Below, we discuss how we go about this task.

3.2.3.1 Possible sources of discrepancy in Run-1 and Run-2

Based on the previous discussions, we note that the ambient vapour isotope values have the maximum impact on the model rain isotope values. This can be shown quantitatively by a multiple regression analysis of rain isotope values with four influencing factors (RH, Temperature, surface δDv and drop diameter) in their normalised forms. The normalised values of the model rain isotope ratios $\delta D_{mod\text{-}rain}$ obtained from Run-2 for the

29 sampling days were regressed with the normalized values of these four variables. We obtain the following multiple regression equation:

$$\delta D_{mod\text{-}rain} = -0.114*RH+0.035*Temperature-0.059*diameter+0.986*\delta Dv \quad (1)$$

This equation indicates that the major influence on the model rain isotope value is from the ambient vapour δDv (with a coefficient of nearly one, meaning +1% change in δDv would result in +1% change in the rain δDv). In contrast, the influence of RH, for example, is only one-tenth (in opposite direction) for the same percentage change. The influences of temperature and size are still less. It is logical to assume that the main source of discrepancy in Run 1 and Run 2 is improper vapour isotope profiles and therefore, for tuning, a change in the vapour isotope value would be the most effective.

It seems that the true profile for a given date does not coincide with the adopted one based on extrapolating to the measured surface value, as assumed by the boundary constraint. In other words, the vapour aloft may not be derived entirely from the surface vapour as measured at our sampling location. One possible explanation could be a significant contribution from the small-scale local surface moisture having a different isotopic composition (evaporation or evapotranspiration from water bodies or trees within a few hundred meters). However, this possibility can be ruled out as a study using satellite data showed that due to high humidity during the monsoon season evaporation/ evapotranspiration (~0.5 mm day^{-1}) adds a negligible amount of moisture compared to the advective flux in this region (Pathak et al., 2014). The search for a true profile in our case is limited by the absence of high-altitude vapour observation of δD and $\delta^{18}O$ values from an independent source or model on a daily scale.

3.2.3.2 Modification of the isotope ratios and Run-3 results

Guided by the regression equations, we tuned the vapour δD and dex input profiles (Run-3) to achieve a reasonable agreement in the rain isotope values for each date (Fig. 5i-5k). The surface δD values were changed by +13.9 to -17.8‰ and the dex values from +3.2 to -17.1‰ while keeping the shape for daily profiles similar to Run-2 (following the adjustment procedure discussed above). Corresponding changes in the vapour $\delta^{18}O$ is from +2.9 to-1.9‰. Most of the changes were small; in the δDv within ±4‰ (discarding six large changes) and in the $d\text{-}excess_v$ within ±3.4‰ (discarding six large changes). These changes improved the results considerably. As a consequence of this tuning, the average d-excess of the surface vapour decreased to ~10.7 ‰ from the measured average surface value of 17.3 ‰. To see these modifications clearly, the Run-3 vapour isotope profiles are shown along with those of Run-2 profiles in Fig. SI-8b-2.

To check the agreement, a two-tailed Student's t-test was done with observed and modelled $\delta^{18}O$, δD, and d-excess values of 29 rain samples after each of the runs. This test shows that the Run-3 model values are close to the observed ones for all three parameters ($\delta^{18}O$, δD, and d-excess) at p=0.05 significance level (see SI-9; Table S9). The outputs of Run-1 and Run-2 agree with each other reasonably well (see Fig. S9-1) for all three isotopic parameters, but they do not agree well with the observed values.

We recognise that it is difficult to validate the vapour δD or d-excess profiles constructed by the above method due to a lack of height-specific observations. However, the available aircraft-based vapour isotope observations suggest that both d-excess and δD values of vapour decrease with altitude and thus provide some

evidential support to the assumed decrease (Sodemann et al., 2017). With the above choice, simulations of rain isotopes improve (Fig. 5i-5k) considerably (both in terms of uncertainty of the slope of the regression line and the correlation coefficient). The average (observation-model) d-excess difference decreases from 2.1 to 0.4. Additionally, there is close match in the Δδ-Δd cross plot (see Fig. 5l).

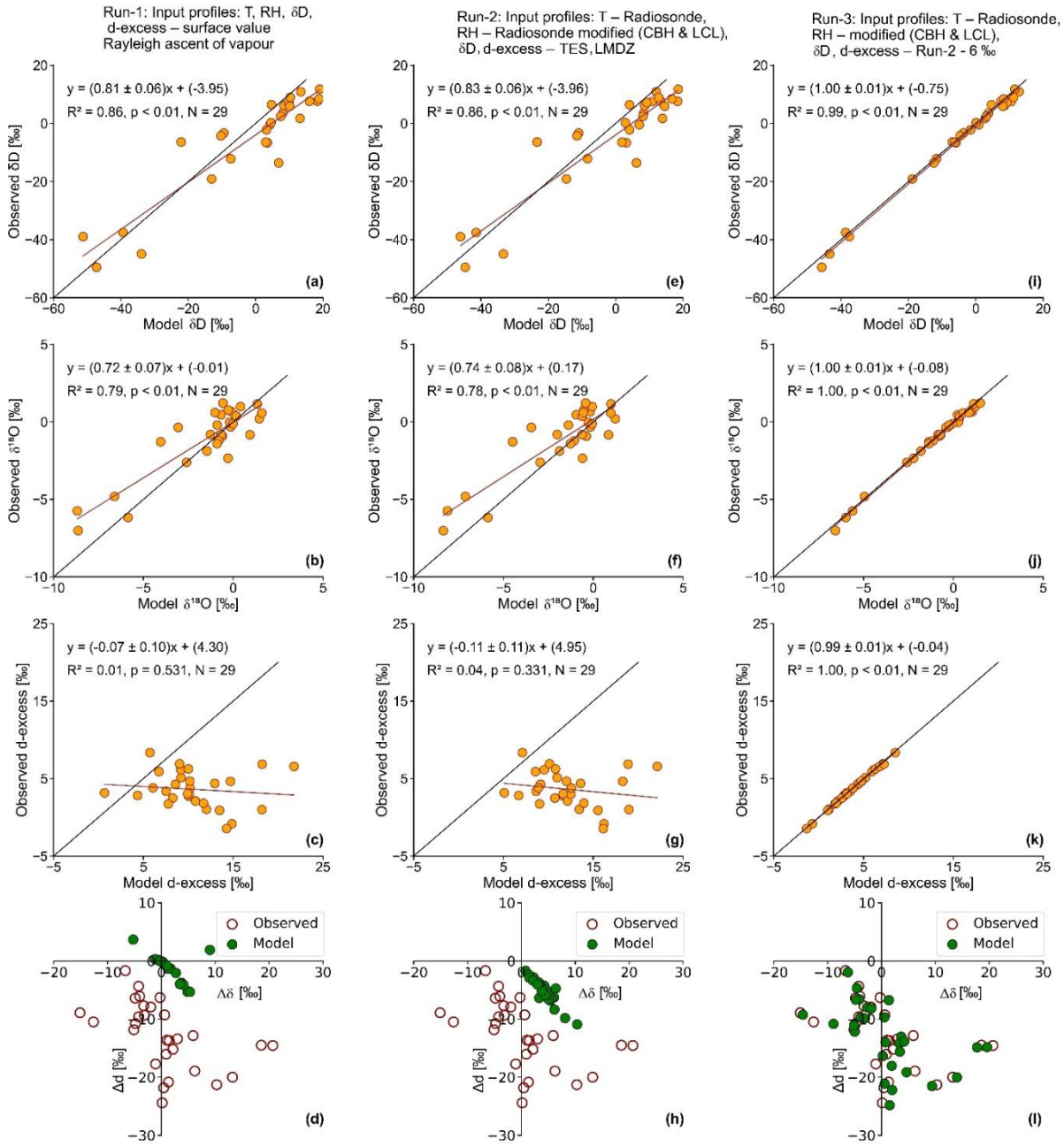

Figure 5. Scatter plots showing observed vs model values for δD, $\delta^{18}O$, and d-excess for various runs (Run-1, Run-2 and Run-3) of BCIM in the upper nine panels. The lowermost three panels show the Δδ–Δd cross-plots for the runs. The input profile sources of T, RH, vapour δD and d-excess used in the model for the three runs are given in the descriptions above. The best agreement between the observed and model values is achieved in Run-3. Run 3 uses the same RH and T as Run 2 but δD, and d-excess values are adjusted by tuning. The average d-excess reduces to ~10.7‰ from the observed value of ~17.3‰ used in Run-2.

The physical basis behind the good agreement in Run-3 is the validity of the assumptions of the cloud microphysics of the BCIM, which calculates the evolution of the raindrops as they fall through the cloud and below-cloud layers. The evolution changes the mass as well as the isotope ratio, finally culminating in the values that we measure on the ground. We think that a reasonable agreement of the isotope values is proof that the assumed cloud microphysics of the BCIM (with all assumed input parameter values) holds good for the drop mass evolution, and therefore the drop evaporation estimated from the same model (see later) can be considered valid.

3.2.3.3 Sensitivity and uncertainty of the model predictions in Run-3

The simulations of BCIM predict the rain isotope ratios based on assumed values of RH, T, drop size and vapour isotope ratios. We did a sensitivity analysis of the model rain composition using Run-1 to study the effects of variation in temperature, relative humidity, vapour isotopes, and drop size, and the results are given in Supplementary Information SI-13. Fig. S13-1 shows that the vapour isotope value is the most important factor in controlling the model rain isotope ratios. For +10% change over the reference value of the parameters, the changes in the rain δD values (in ‰) are: +7.6 (for δDv), -4.1 (for RH), +2.6 (for T) and -0.4 (for diameter).

We also determined the uncertainty of the model predictions of dD (rain) and d-excess (rain). Using the Run-3 model output values, we obtained a multi-parameter regression equation for δD (rain) as a function of the four variables (vapour isotope, relative humidity, temperature, and drop diameter) δDv, RH, T and D. With given inputs of errors in δDv, RH, T and D, the uncertainty in the rain isotope value δD_{rain} is 3.5 ‰. Using a similar exercise for the d-$excess_{rain}$ we obtain uncertainty for the d-$excess_{rain}$ as 2 ‰. The details of the calculations are given in SI-14.

4. Discussions

4.1 Influence of local meteorological parameters on isotopes

Water isotopes in the tropics often vary with rainfall, humidity, and temperature (Dansgaard, 2012; Lee and Fung, 2008). Scatter plots between the vapour d-excess values and local meteorological parameters such as rainfall amount, relative humidity, specific humidity and temperature are shown in Fig. S10-1. The d-excess of vapour shows only a marginal positive correlation with temperature (R^2=0.16; p-value=0.03; not significant) and a small negative correlation with relative humidity (R^2=0.22; p-value=0.01; marginally significant).

It is known that temperature and relative humidity of air have opposite controls on raindrop evaporation (Lee and Fung, 2008; Stewart, 1975). If the drop in evaporation affects the rainfall significantly, we should have seen some relation between the rainwater isotopes and rainfall. The absence of correlation in tropics is also found in several other studies (Chakraborty et al., 2016; Moerman et al., 2013; Vimeux et al., 2011). Even though a relation with rainfall is absent, a correlation is often found with the regional convective activities (Kurita, 2013; Lekshmy et al., 2018). Risi et al. (2023) have noted that in the tropics, most of the precipitation falls under deep convective systems (see Section 3.1 and Fig. 2), which are controlled by various microphysical processes (like rain evaporation, diffusive liquid-vapour exchanges, and mesoscale downdrafts) connected through mesoscale circulations. These processes probably override the effect of surface meteorological parameters in our region.

552 **4.2 Rain-vapour isotope exchange and rain evaporation**

553 An increasing trend (13 ‰ to 30 ‰) in the vapour d-excess values associated with a decrease in the
554 $\delta^{18}O$ values with the progress of the monsoon (Fig. 2b) could be ascribed to significant recycling of the moisture
555 with contribution from some evaporative sources. Risi et al. (2023) have discussed the possibility of down-
556 drafted vapours as the source of such anomalously low isotope ratios in the case of Sahelian squall lines. Earlier
557 studies over some Indian sites have shown that changes in moisture sources are often associated with a
558 concomitant change in isotope values in rain and vapour (Deshpande et al., 2010; Midhun et al., 2018). We
559 investigated the possibility of this by forty-eight hours of air-parcel back trajectory analysis (Fig. S4-1), which
560 shows that moisture was derived mainly from the Arabian Sea. However, this does not rule out the possibility of
561 minor evaporative contributions from continental moisture sources enroute or down-drafted moisture
562 characterised by low isotope ratios and high d-excess values (Risi et al., 2010).

563 The microphysical process of evaporative exchange during the fall of raindrops causes isotopic
564 enrichment in the rain. Though important, raindrop evaporation cannot be easily quantified. As discussed
565 before, evaporation is reflected in higher δ-values and lower d-excess values (mean~2 ‰) of the rain samples.
566 Froehlich et al. (2008) used d-excess values of precipitation in the Alpine region to derive the extent of
567 evaporation using assumed end-member values of the regional vapours.

568 Any isotope exchange between the rain and ambient vapour would result in correlated changes. A
569 strong correlation between rain and vapour $\delta^{18}O$ values is indeed found (Fig. 6a; R^2=0.7, $p < 0.01$, n=29),
570 suggesting a connection between them. Sinha and Chakraborty (2020) also found significant positive relations
571 (R^2>0.8) between rain and vapour $\delta^{18}O$ values over Andaman Island. However, they did not find any anti-
572 correlation between rain $\delta^{18}O$ and rain d-excess, as found here (Fig. 4b). The current study exhibits a reasonable
573 anti-correlation between the differences in d-excess ($\Delta d\text{-excess}_{r\text{-}v}$) and $\delta^{18}O$ ($\Delta\delta^{18}O_{r\text{-}v}$) of rain and vapour (the
574 subscript r-v indicates Rain isotope minus Vapour isotope) (Fig. 6b). This would be expected if evaporation of
575 rain contributes a significant amount of vapour because the generated vapour is lower in $\delta^{18}O$ but higher in
576 d-excess compared to the rain.

577 As raindrops evaporate, the newly formed vapour may get down-drafted to lower levels, and therefore,
578 the two phases at the ground level would exhibit opposite changes. However, in the case of tropical
579 precipitation, we do not expect a substantial contribution from rain evaporation to the ambient vapour because
580 the latter is a large reservoir. It has been shown in several earlier studies that the total rain is derived from only a
581 few percent of the overhead vapour mass (Pathak et al., 2014; Rahul et al., 2016). Earlier studies have also
582 shown that vapour d-excess values do not exhibit any systematic change in central or southern WG stations,
583 although, surprisingly, their rain $\delta^{18}O$ values exhibit slight but gradual depletion (1 ‰ to -10 ‰) in the later part
584 of the monsoon (Lekshmy et al., 2018; Rahul et al., 2016). The negative correlation found in this study suggests
585 that the ground-level vapour gets a significant contribution from drop evaporation. How can moisture generated
586 by drop evaporation over the falling path contribute to the ground-level vapour? This is possible when there is a
587 strong downdraft associated with intense monsoon rains (Risi et al., 2023). In a modelling study, Mandke et al.
588 (1999) pointed out that deep convective cloud systems contain both upward and downward components. The
589 downward motion is driven by the evaporation of falling precipitation and the dragging of the ambient air and
590 vapour by big droplets. This downdraft brings moisture down from above and increases the vapour d-excess at
591 the surface (Risi et al., 2010; Kurita, 2013; Aemisegger et al., 2015). The existence of drop evaporation is

592 further supported by a relation between Δd-excess$_{r-v}$ and surface relative humidity (RH; R^2=0.31; Fig. 6c). The
593 difference between rain and vapour isotopes is more in lower RH and less in higher RH, as expected (Stewart,
594 1975). A similar analysis (Xing et al., 2020) in China also found that the change in isotopic composition is large
595 when RH is less than 60 %.
596

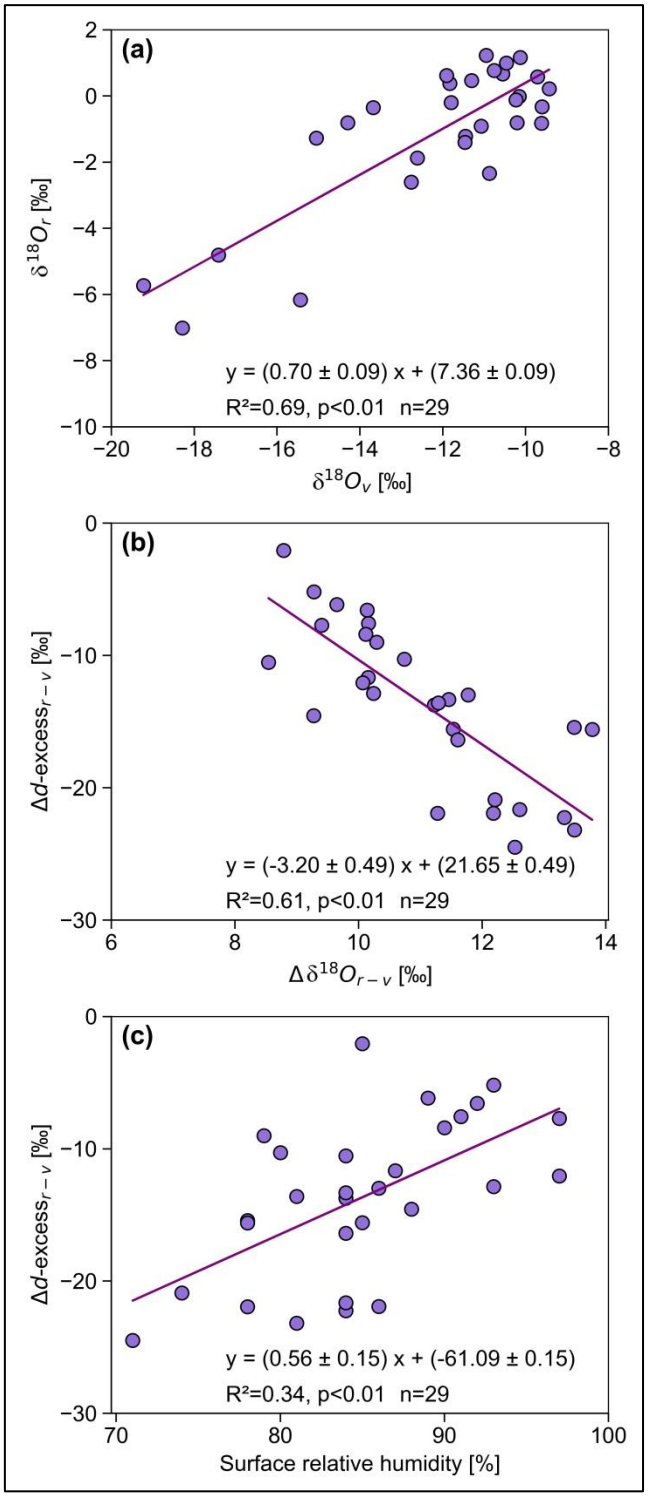

597
598 **Figure 6.** The correlations between **(a)** δ^{18}O of rain (δ^{18}Or) and δ^{18}O of vapour (δ^{18}Ov) at the ground level; **(b)** the
599 difference in d-excess of rain and vapour (Δd-excess$_{r-v}$) and δ^{18}O ($\Delta\delta^{18}O_{r-v}$) showing that the rain value is lower in d-excess

whereas it is higher in $\delta^{18}O$; **(c)** difference in the d-excess of rain and vapour (Δd-excess$_{r-v}$) and ground level relative humidity (RH).

Falling raindrops and the water vapour in the atmospheric column constitute an interacting two-phase system, especially below the cloud base. On the way down, the water molecules are constantly exchanged between these two phases depending on the ambient RH and temperature. This makes the system evolve towards an isotopic steady state. The difference between isotopes (δD and d-excess) of vapour in equilibrium with raindrops and the observed surface vapour (defined as $\Delta\delta$ and Δd, respectively) is useful to quantify the departure from equilibrium. Graf et al. (2019) demonstrated the importance of a $\Delta\delta$-Δd plot to represent the effect of sub-cloud processes, such as evaporation and equilibration, which influence the water isotopes. The time series of $\Delta\delta$ values (Fig. 7a) for the Pune precipitation samples shows that the values varied between -15 ‰ and 21 ‰. For Δd, the time series shows negative values in all cases (ranging from -2 to -24 ‰). The close-to-equilibrium samples correspond mostly to the high-humidity period in July (Fig. 7b). Fifteen samples indicate the influence of below-cloud evaporation with positive $\Delta\delta$ values associated with strongly negative Δd values (up to -20 ‰).

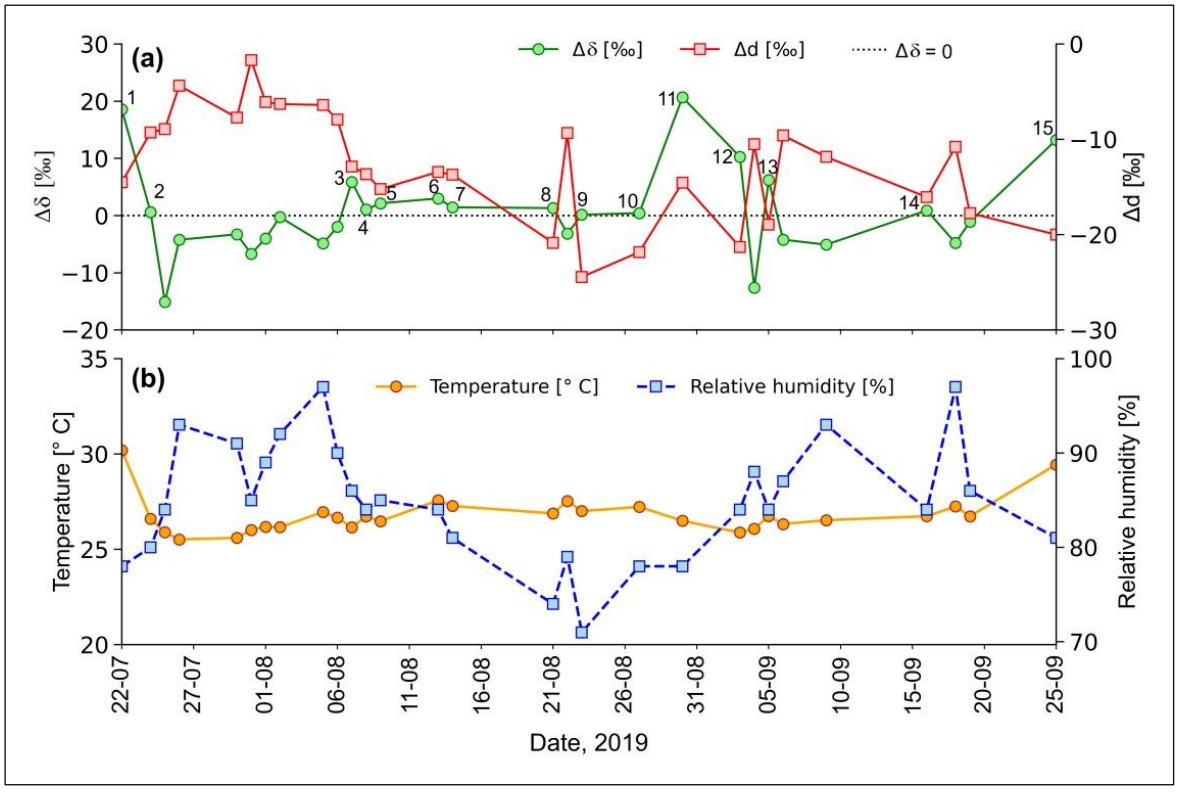

Figure 7. (a) Time series of $\Delta\delta$ and Δd of the rain samples collected during 2019 monsoon (July to September) in Pune. $\Delta\delta$ and Δd values (total points=29) denote rain-equilibrated vapour isotope minus the surface vapour isotope. The blue dotted line indicates $\Delta\delta$=0. All data points where $\Delta\delta$>0 are marked with numbers totalling 15, **(b)** Time series of daily average surface temperature and relative humidity recorded at IMD observatory at Pune.

A $\Delta\delta$-Δd scatter plot based on these observed data (Fig. 8) shows that none of the rain samples is in equilibrium with the corresponding ground-level vapour. If the equilibrium pertained, the points would plot at

the origin. 15 sample points fall in the lower right quadrant of the diagram, where the raindrop evaporation is relatively more significant, as per Graf et al. (2019). We note that the observed rainfall amount was low (less than 5 mm) for these samples, which is consistent with a substantial evaporation effect. 14 samples have negative Δδ and Δd values, indicating incomplete equilibration with near-surface vapour. The crucial driving factors for below-cloud processes seem to be the size of raindrops and the intensity of precipitation. This is primarily because raindrops with larger diameters correspond to increased intensity and have shorter residence times in the atmospheric column. As a result, they experience reduced evaporation while descending toward the ground. However, the drop size in this study was not derived by an independent method. They were based on rain rates or precipitation intensity through M-P relation and are not independent. A clearer demonstration of the relation between rain rate and drop size was provided by Law et al. (2021), who showed that higher rainfall intensities are characterised by closer distances among raindrop particles. This results in higher chances for smaller raindrops to collide and to coalesce into larger droplets before falling from the cloud. We note that our data is consistent with their conclusion.

Distribution of points in the Δδ-Δd plot (Fig.8) shows that 10 samples with <5mm/day rain rate fall in the lower right quadrant compared to 5 in the left quadrant. This suggests that drop evaporation is a dominant process in low rainfall events (where smaller drop sizes dominate). To see the rainfall or drop size effect more clearly the size of the points was characterised in terms of drop size, and the colour of the points was varied, indicative of rainfall (Fig. 8). It seems that larger drop size points with higher rainfall are always in the lower left quadrant. This indicates that in such cases, the memory of the isotopes is partly retained even after sub-cloud evaporation due to larger sizes. The 29 sampling points are nearly equally distributed in the two quadrants, suggesting an equal number of equilibration-dominant and evaporation-dominant rain events. It is to be noted that deep convective rains during the monsoon exhibit significantly higher mass-weighted diameter compared to shallow convective rains or stratiform rains (Kumar et al., 2025). The five big diameter points in the lower left quadrant correspond to such cases of deep convection.

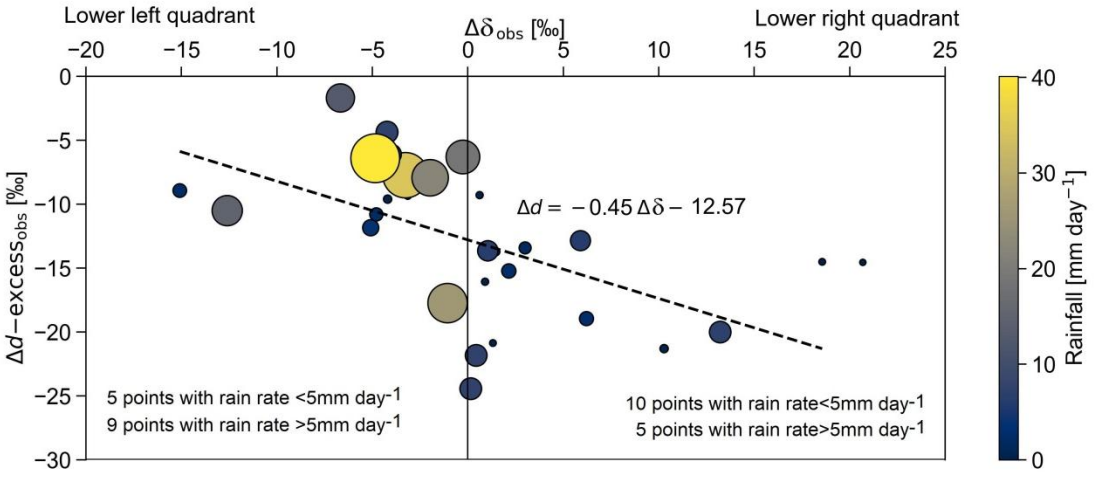

Figure 8. The Δδ-Δd plot based on observed values for various rain rates. The size of the sample circles indicates drop size; their variation is also associated with the rain rate (scale on right). We note that most of the 4th quadrant (lower left) points are of bigger size and those in the 3rd quadrant (lower right) are of small size. The line shows a good fit to the data with a

653 slope of -0.45.
654
655 The regression line in the Δδ-Δd cross plot (Fig. 8) based on all 29 observed values has a slope of -0.45
656 based on Bootstrap analysis (See SI-11). This is more than the slope of -0.30 reported by Graf et al. (2019) for
657 their study area, Zurich, Switzerland. Their study was based on short-time intra-event samples (covering about
658 16 hours and each rain sample being collected for 10 to 15 min) in a mid-latitude region, whereas 29 daily
659 samples in a tropical region (covering a few months and each rain sample being collected for 24 hours) are used
660 in the current study. A set of complex processes operates to dictate the value of the slope, and Graf et al. (2019)
661 pointed out that the slope could represent a balance between below-cloud evaporation and equilibration. They
662 suggested that it would be insightful to explore the slope for other climatic regions, hinting that the slope will
663 help assess the evaporation magnitude. A quantitative estimate of the evaporation fraction can be obtained from
664 BCIM by using the mass loss discussed later in section 4.3.
665
666 Graf et al. (2019) showed that at high humidity (lower evaporation), the change of Δd is negligible,
667 leading to a lower slope. Conversely, when the temperature is higher, the slope is higher due to higher
668 evaporation. The slope is essentially due to a differential effect in evaporative fractionation. Evaporation
669 decreases rain d-excess but increases rain δD. However, the magnitudes of these changes (negative for d-excess
670 and positive for δD) are not the same. Fractionation values (involving equilibrium and kinetic factors) show that
671 the change in δD is larger compared to that in d-excess (about 30% of the δD change, considering the absolute
672 values). This is because in evaporation, the kinetic effect operates in addition to the equilibrium fractionation,
673 and that has more influence on δD compared to $\delta^{18}O$. If the evaporation is higher (due to higher temperature and
674 lower RH), the deviation from the equilibrium fractionation line will be more, and the slope will be higher. In
675 the frontal systems of Switzerland, the temperature was about 12°C and RH about 80% (Graf et al., 2019)
676 compared to Pune, where T was about 25° C and RH about 85%. We see that RH is nearly similar, but the
677 temperature is much higher in Pune. The normalized multiple regression equation of evaporation fraction as a
678 function of RH, T and size (diameter D), given below, shows that temperature plays an important role (nearly as
679 much as RH for evaporation):
680
681 Evaporation Fraction (norm) = -0.329* RH +0.370* Temperature -0.665* Diameter (2)
682
683 For the larger values of Pune temperatures, we expect more evaporation, which leads to the higher
684 slope value of -0.45 for Pune compared to -0.30 for Zurich. The multiple regression equation for evaporation
685
686 **4.3 Estimate of raindrop evaporation and its uncertainty**
687 The output of BCIM in Run-3 predicts that the mass of the drop reduces as it falls. The ratio of final
688 mass to the initial mass (m/m_o) can then be used to estimate the fractional mass loss suffered by the drop on its
689 way down. The difference ($1-m/m_o$) represents the effective rain evaporation. With this definition, a time series
690 of evaporation values (Fig. 9a) shows variation from 4 % to 60 % (average ~23 %). As expected, drop
691 evaporation is inversely related to the surface humidity (Fig. 9b) and drop diameter (Fig. 9d) but directly
692 proportional to the temperature (Fig. 9c).

The evaporation was particularly high (60 % and 59 %) on 22 July and 21 August when humidity was relatively low (78 % and 74 %), and the temperature high (30° C and 27° C) and the diameter small; the combined effect resulted in high evaporation (Fig. 9a). The deduced evaporation fractions are moderately high (23±16) % which is consistent with the observed anti-correlation between d-excess and $\delta^{18}O$ of rain samples (Fig. 4b).

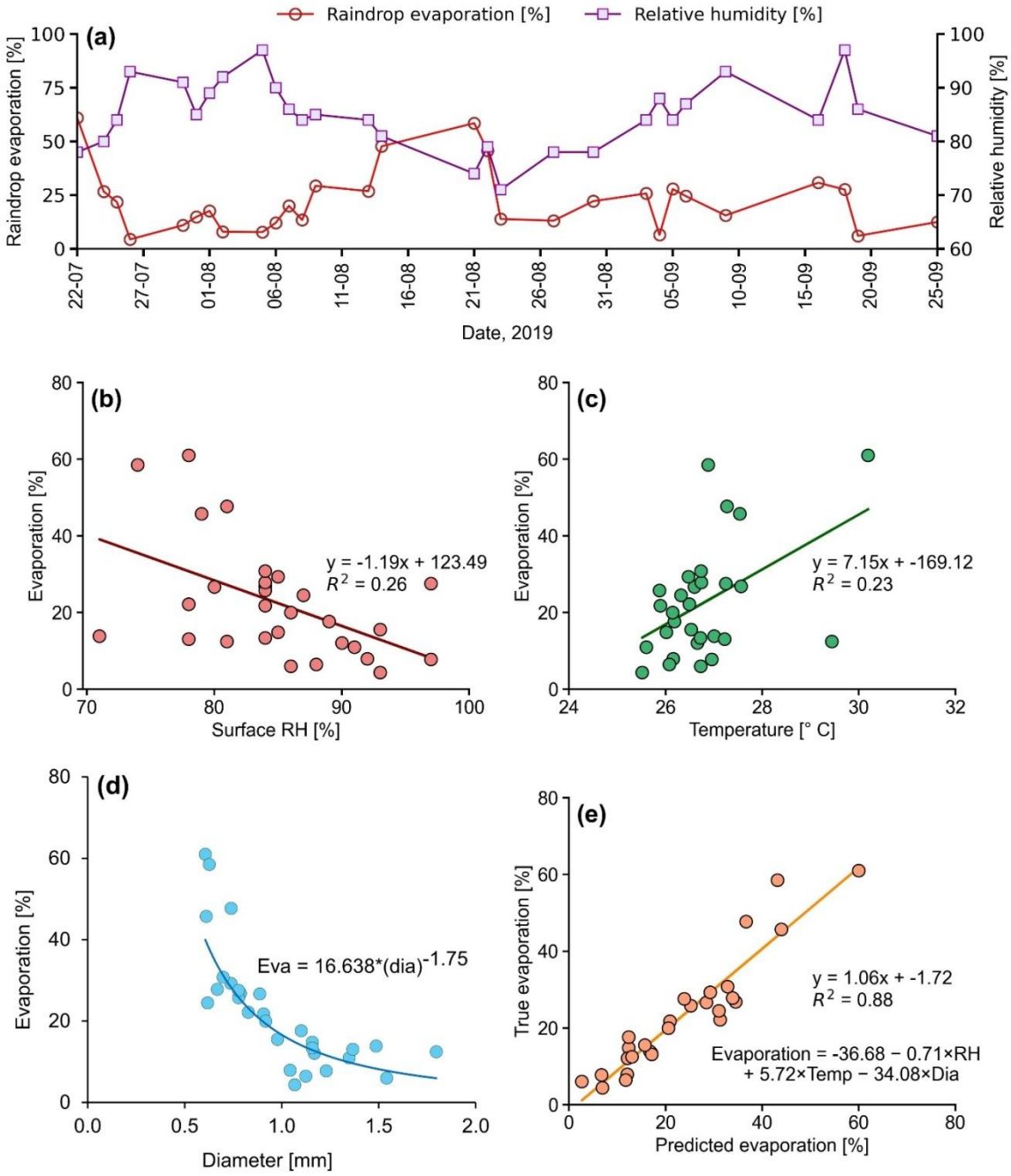

Figure 9. (a) Time series of raindrop evaporation using BCIM simulation (Run-3) and surface relative humidity. The regression between raindrop evaporation fraction with **(b)** RH, **(c)** temperature, and **(d)** drop diameter. **(e)** Multiple regression analysis yields the equation shown in the inset. The regression equation prediction of evaporation explains nearly 88% of the variance.

Among the controlling factors, the temperature does not vary much (26.8±1.0 °C), while for RH, the variation is slightly larger (85±6 %). The diameter variation, on the contrary, is much higher, at about 30% (1.0±0.3 mm) and has a higher impact on the evaporation. The multiple regression equation (using unnormalized variables) can be used to estimate the error in drop evaporation, knowing the uncertainties in RH, T and drop diameter and using the partial regression coefficients as partial derivatives. The Evaporation Fraction (EF) was regressed with RH (in %), Temp (in °C) and the drop size D (diameter in mm). and yields:

$$\text{Evaporation Fraction} = -36.68 - 0.71*RH + 5.72*T - 34.08*D \quad (3)$$

Using the standard quadratic formula for error (Farrance and Frenkel, 2012) we obtain:

$$\sigma(EF)^2 = (\partial EF/\partial RH)^2 * \sigma(RH)^2 + (\partial EF/\partial T)^2 * \sigma(T)^2 + (\partial EF/\partial D)^2 * \sigma(D)^2 \quad (4)$$

Where σ denotes the uncertainties in EF, RH, T and D, and the quantities in brackets express the partial derivative of EF with respect to the variable. The uncertainties associated with RH and T in Radiosonde observations are 8% and 0.3° C (Sapucci et al., 2005), and the uncertainty of the diameter is 20%. Using the above equation, the error σ(EF) varies from 7.4 to 13.8 % (for EF values from about 5 to 61%). The mean error is ±10%.

4.4 Evaporation and rainfall relation

Evaporation fraction plotted as a function of rainfall (Fig. 10) shows that the two parameters are related by a power law. For a smaller rainfall range (less than 5 mm day^{-1} to 10 mm day^{-1}), the evaporation affects the rainfall significantly. The reason is that smaller rainfall is usually associated with smaller drops, which are very sensitive to evaporation, resulting in a power law.

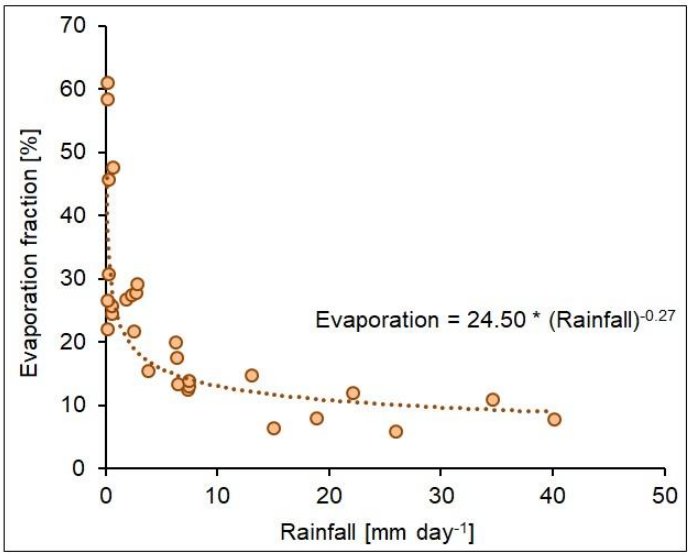

Figure 10. Scatter plot shows relationship between the estimated drop evaporation and rainfall in Pune. The black dashed line indicates the best-fit power law. Higher rainfall implies drops of bigger size and hence lower evaporation fraction.

It is instructive to compare our results to the evaporation estimates obtained in similar studies carried

734 out in other climatic regimes. Sarkar et al. (2023), in a steady state one-dimensional model study of rain in the
735 North Atlantic Trade Wind region (Barbados), found a high value of 63% (63±23 %) for raindrop evaporation
736 (using radar reflectivity data on rain evaporation flux), which is three times more than our average value of 23%
737 (23±16 %). We have only four high evaporation days (more than 45%) out of 29 sampling days. The reason for
738 the large difference in Pune evaporation from Barbados is possibly due to a large difference in drop size and
739 RH. A comparison reveals that in Barbados, the drop sizes were much smaller (from 0.1 to 0.6 mm) in
740 comparison to ours (from 0.61 to 1.80 mm). Their drops were so small in some cases (smaller than 0.3 mm on 4
741 February 2020), that the drops completely evaporated (evaporation ~ 100%) during the fall. In addition, in their
742 sampling region, the RH was lower, ranging from 65% to 80%, compared to ours (74% to 97%). Smaller drop
743 size and lower RH lead to higher raindrop evaporation. We also note that their drop sizes varied over a wider
744 range, leading to a larger variability compared to our study.
745 In a similar study as here, rain and vapour isotopes were measured in a cold-front passage over Zurich
746 during 19-25 July 2011, and the data were interpreted by an isotope-enabled regional weather prediction model
747 COSMOiso (Aemisegger et al., 2015). The authors showed that by switching off the raindrop evaporation, the
748 rainfall increased by about 75% because the cooling induced by evaporation causes diminished convective
749 activity. The estimated average evaporation in their study was about 40%. This value is nearly twice our value.
750 The reason is probably a smaller drop size and lower RH; as stated in their paper: "weak rainfall intensities
751 (small droplets and thus lower falling velocities), and possibly lower relative humidity in the air column could
752 have contributed to the evaporative enrichment of precipitation".
753
754
755 **5 Summary and Conclusions**
756 **5.1 Key Findings**
757
758 We analysed isotope ratios of daily rain and atmospheric vapour samples collected from the surface level at
759 Pune, a tropical rain shadow region in Western India, during the summer monsoon season (June-early October)
760 of 2019. The seven major findings of our study are listed below:
761

762 1. The vapour isotopes show considerable temporal variation (with $\delta^{18}O$ from -19.2 ‰ to -9.4 ‰ and δD from -
763 123.7‰ to -63.4‰). The corresponding rain isotope variations are smaller, $\delta^{18}O$ from -7.5 ‰ to 1.2 ‰
764 and δD from 58.9‰ to 11.8‰. The rain isotopes are not in equilibrium with the ground vapour. In most
765 cases, the rain $\delta^{18}O$ values are higher than expected from equilibrium with the ground vapour (by about 2‰
766 on average). In contrast, the δD values are only a little higher, on average, by about 0.7‰; but there are
767 some extreme values, some are higher by about 20 ‰ and some are lower by about 15‰. The deviation
768 from equilibrium is caused by fractionation that raindrops suffer through evaporative exchange (involving
769 equilibrium and kinetic fractionations) during their fall. This fractionation changes the isotope ratios of
770 droplets that originated at heights of 830 ±70 mbar.

771 Interestingly, considering the whole monsoon season of 2019, there were four events extending over a few
772 days when both rain and vapour isotope ratios were considerably lower (for example, rain values were less

than the mean - 0.5 standard deviation, with $\delta^{18}O$ less than -2.6 ‰). These events seem to be related to regional meteorological characteristics (see below).

2. We note that the low rain isotope events are synchronous with negative OLR anomalies. Negative OLR anomalies during the Indian summer monsoon are usually associated with large-scale convections (Sengupta et al., 2020). The intense convective events, indicated by these anomalies, lift the air parcels to higher altitudes where the ambient vapour isotope ratios are highly depleted. Droplets formed from these vapours are correspondingly depleted. The drop isotope values may be so negative that even evaporative exchanges may not alter/increase their values much, especially if they are of big size. The high negative isotope values of ground vapours could be due to downdrafts associated with strong evaporative cooling of raindrops. The proposition that air parcels are lifted to higher altitudes during intense convective events is supported by the presence of a second CLWC peak (about 550 mb; see Fig. 3) for 19, 25, 27 Sept, 2019 when the rain and vapour isotopes were both highly depleted (rain δD values are -39 ‰, -49 ‰ and -59 ‰ compared to the average of -7‰) and associated with the negative OLR anomaly (Fig. 2). It seems that on those days intense convection lifted the moist air parcels to about 5.5 km which were responsible for high second CLWC peaks.

3. A gradual increase in the d-excess values of vapour and a small but notable decrease in $\delta^{18}O$ values in the later part of the monsoon (after mid-August) are observed. The high vapour d-excess in September is especially noticeable. We also find a strong anti-correlation between vapour $\delta^{18}O$ and vapour d-excess values. Such anti-correlation usually indicates a significant contribution to the ground vapour from evaporative sources, which, in our case, accumulated slowly with the progress of the monsoon. Pathak et al. (2014) also found a higher precipitation recycling ratio, that is, the ratio of recycled precipitation to total precipitation in central India, at the end of the monsoon (September). In contrast, the rain d-excess values are not significantly different because there is no such cumulative effect for the rain.

4. The above observations suggest increased vapour contribution from evaporation of raindrops and/or from local evapotranspiration (ET) sources, especially increasing with the monsoon progress. However, vapour supply from surface sources cannot be a large factor. Pathak et al. (2014) showed that for central India, the ET contribution increases with the progress of the Monsoon but can at best account for 5 to 10% of the vapour mass. Therefore, we strongly believe that the downdraft of depleted vapour (and not local supply) is the main source of low $\delta^{18}O$ (and high d-excess) surface vapour (Risi et al., 2023). The depleted vapour in the sub-cloud region can originate from raindrop evaporation, and such vapour can be downdrafted by the drag of the falling raindrops. However, a single-column model like BCIM cannot capture this process.

5. In the Δδ-Δd (Δ indicates the isotope ratio of vapour in equilibrium with rain minus the ambient vapour isotope ratio, following Graf et al., 2019) cross plot, about half of the data points lie in the lower right quadrant, which signifies the importance of raindrop evaporation over Pune and the adjoining region during our study period. The distribution of points in this quadrant is indicative of drop evaporation, but this fact alone cannot quantify the magnitude. We determined the slope $\Delta d/\Delta\delta$ of the points in the cross plot and found a value of -0.45, which suggests that the evaporation in Pune was intense. This is because a higher

slope in the cross plot is caused by a relatively magnified effect of d-excess difference between the rain (and corresponding equilibrated vapour) and the ambient vapour caused by a larger evaporation. A comparison can be made with the study of Graf et al. (2019), who found a lower slope at a value of -0.31 for Zurich. The slope is essentially due to a differential effect in evaporative fractionation. Evaporation decreases rain d-excess but increases rain δD. However, the magnitudes of changes, negative for d-excess and positive for δD, are not the same. Fractionation values (involving equilibrium and kinetic factors) show that the change in δD is larger and that in d-excess is lower (about 30% of the δD change, considering only the absolute values for the changes). This is because in evaporation, the kinetic effect operates in addition to the equilibrium fractionation and that has more influence on δD compared to $\delta^{18}O$.

The factors that influence evaporation are RH, T and drop diameter. As mentioned before, their relative influence is expressed by a multiple regression equation (EQ. 2) using the normalized values of the variables. If the evaporation is higher (due to higher temperature and lower RH) the deviation from the equilibrium fractionation will be more, and the slope will be higher (Gat, 1996). In the frontal systems of Switzerland, the temperature was about 12°C and RH about 80% (Graf et al., 2019) compared to Pune, where T was about 25° C and RH about 85%. Since we know that temperature plays an important role (as much as RH) for evaporation (see coefficients of the normalized evaporation equation, 0.370 against -0.329 in the multiple regression equation (EQ. 2) for the large increase in Pune temperature, we expect more evaporation. This factor possibly leads to a higher slope value of -0.45 for Pune compared to -0.31 for Zurich.

6. To quantify the sub-cloud processes altering the rain isotope values, we used the Below Cloud Interaction Model BCIM. Upon reasonable tuning of the input parameters, we obtained a notable agreement between the observed and model rain isotope values at the ground level.

7. Since the BCIM is found to be applicable to our study area, we estimate the raindrop evaporation parameter from the model output. An event-to-event quantification of raindrop evaporation is the key finding of our study. The model gives a net reduction of the drop mass at the ground level, and we can define the relative reduction ($1-m/m_o$) as a measure of the effective rain evaporation. Using this innovative technique, the model shows that, on average, about 23 % (varying from 4 % to 60 %) of the drop mass evaporates in the sub-cloud layer. There are four abnormally large values (46, 48, 58, and 60 %) of evaporation. The largest value is probably due to low RH (~78%) and high temperature on that day, but as for the other days, probably a combination of smaller drop size and lower RH played a role. Excluding these four values, the average evaporation is 18±8 % (range of 4 to 30 %).

5.2 Limitations and uncertainty of the derived parameters

The isotope technique and the BCIM, which we used, are associated with the following limitations:

(a) We used TES satellite data averaged over 2005-2009 to guide our choice of vapour isotope profiles, but the year of analysis was 2019. In this matter, there is no way to ascertain the degree of deviation of the true profile from the adopted ones in Run-2 and in Run-3.

(b) There are limitations on the use of RH and T from radiosonde. On operating days, the radiosondes are usually launched at 00Z and 1200Z in Pune. Due to operational challenges, these measurements are not generally carried out when there is rain. The radiosonde data for Pune are expected to be reasonable for use in the model if we can at least show that the difference between the two consecutive available measurements is not large. The difference between RH (ΔRH) and temperature (ΔT) measured at 1200Z and 00Z is plotted against height in Fig. SI-12-1 for the 29 days that are considered in the BCIM runs. The figure shows that the ΔRH values are within ± 10% on most days (~80% of the total sampling days) and ΔT values are within 2°C. This is expected as those parameters over western India do not vary much during the Indian Summer Monsoon (Pathak et al, 2014). We need to check how serious these differences are in the context of their use in the model. We have shown through sensitivity analyses and two multiple regression analyses that the effects of the daily scale variation in RH and T on model rain isotope values and evaporation fraction are not significant. We also demonstrate further that the RH and T data from the radiosonde used in this study is more reliable than the same obtained from any satellite datasets.

The $\delta^{18}O$ profiles were adopted based on the δD and $\delta^{18}O$ profiles obtained from the LMDZ model. As noted, this did not give us good agreement with the observations. Run-2 uses radiosonde for the thermodynamic profile, δD from satellite data from 2005-2009, and $\delta^{18}O$ from the d-excess of the GCM extrapolated to the observed vapour measurement at the ground. We realize that there are major concerns with these inputs coming from different data products that all have different spatial/temporal scales and measurement principles. But we would like to emphasize that when any atmospheric model is initialised, by necessity, the input parameters from various sources are used, which may have different spatial and temporal resolutions and measurement principles. Moreover, datasets from various sources are also utilized in the atmospheric model across different parametrization schemes and nudging. Nudging is a well-known technique where the model values are adjusted to accord with the observed values, where available. For example, Graf et al. (2019) used point-based radiosonde RH and T observations, as well as isotope outputs from a limited-area model (Pfahl et al., 2012; Villiger et al., 2023), with a km-scale resolution, as input to BCIM. These two datasets have different scales and measurement principles. Guided by their argument, we have taken the Radiosonde profiles of each sampling day as our choice and adjusted the lowermost parts to match the measured RH and T values at the ground taken from the IMD.

(c) The isotope profiles were constructed using ground observations as boundary values. However, this also resulted in a mismatch with the observed values (in Run-2), and we had to tune to lower $\delta^{18}O$ values and higher d-excess values to achieve good agreement. It should be mentioned here that Risi et al. (2023) also discussed a similar idea in their study of water isotopes in tropical squall

lines, that convective downdrafts can introduce depleted vapour produced by rain re-evaporation in the boundary layer. Another limitation is that the vapour samples were collected for a duration (about a few hours) that did not coincide exactly with the longer rain collection period (about 24 hours).

(d) The raindrop formation height was assumed to be the CLWC peak level for all rainy days, and the drops were all introduced at that level. However, it is well known that raindrops do not all form at the same height, even on a single day. With this assumption, we are neglecting alterations in isotope ratios produced inside the cloud by various microphysical processes.

(e) Although some studies pointed out that collision-coalescence is an important warm rain process that occurs in various rain shadow regions of India (Padmakumari et al., 2024), including those in the Western Ghats (Konwar et al., 2014), BCIM neglects the process while estimating rain isotope values. We think that this may introduce some error in rain evaporation estimation, but that cannot be quantified in the present study. Since collision coalescence is a non-fractionating process, the effect would be only through drop size modification. Therefore, the isotope effect would be a secondary effect and is expected to be small.

(f) We provide uncertainty estimates of the model rain isotope values (δD_{rain}, $dexcess_{rain}$) in section 3.2.3.3 and raindrop evaporation fractions in section 4.3. Several assumptions are required to calculate the uncertainties in these parameters. The uncertainty values for δD_{rain} is 3.5 ‰, for $dexcess_{rain}$ it is 2 ‰, and for drop evaporation it is 10%.

5.3 Impact of evaporation on rainfall and heat budget

Presence of evaporation of raindrops during the Indian Summer Monsoon has been postulated earlier in several theoretical models, but this study provides, for the first time, a quantitative estimate of rain evaporation on a day-to-day basis in the monsoon season using combined rain and vapour isotope data. We found that about 25 % raindrop evaporation occurred in 2019 monsoon season in the highly humid Pune region. The average seasonal rainfall in Pune is about 55 cm (during monsoon), and if ~25 % of this is evaporated, it would mean considerable cooling of the boundary layer, leading to localized downdrafts, formation of cold pools, and changes in atmospheric stability. Cooling can also hinder efficient formation of convection (Hwong and Muller, 2024) and can have a large effect on the precipitation patterns in the tropics (Bacmeister et al., 2006; Sarkar et al., 2023). Given the large share of precipitation recycling found in this study for Pune, the question arises: how large is the precipitation recycling at larger scales, i.e., regional or continental scales, as well as in other seasons over India. We need to have a comprehensive program for carrying out such analysis, aided with appropriate BCIM input parameters, to understand the evaporation of raindrops over various climatic subdivisions in India. Moreover, high-frequency observation of vapour and rain isotopes would be useful to quantify this fraction during various convective events associated with low-pressure systems during the monsoon. A quantitative estimate of raindrop evaporation would be of great help in modelling the energy and moisture budget during the monsoon season.

Data Availability

Observed rain and vapour isotope data are available upon communication with the corresponding author. The upper-air radiosonde measurements were obtained from the University of Wyoming repository

(http://weather.uwyo.edu/upperair/sounding.html). The daily gridded data (zonal and meridional wind, specific humidity, air temperature, and cloud liquid water content) are available from the European Centre for Medium-Range Weather Forecasts Reanalysis (ERA-5; https://www.ecmwf.int/en/forecasts/datasets/reanalysis-datasets/era5). The rainfall data (cumulated over 24 hours) are obtained from the Pune observatories of the IMD (available at the National Data Centre (www.imdpune.gov.in/ndc_new/ndc_index.html)). Apart from daily rainfall, hourly rainfall data and daily average temperature and relative humidity data for the Pune observatory were also obtained from the IMD using the above link. The datasets for 48 h air mass back trajectory analysis at 850 mb pressure level are obtained from the NOAA Hybrid Single-Particle Lagrangian Integrated Trajectory (HYSPLIT) model (https://www.ready.noaa.gov/HYSPLIT.php). We received daily outputs of LMDZ isotope-enabled GCMs, which were provided by Dr. Camille Risi by personal communication. The Interpolated Outgoing Longwave Radiation (OLR) data from NOAA (https://psl.noaa.gov/data/gridded/data.olrcdr.interp.html) is used in this study. Tropospheric Emission Spectrometer (TES) Level 2 (Nadir-Lite-Version 6) retrievals of HDO and H_2O profiles for the available period (2005–2007; https://tes.jpl.nasa.gov/tes/data) are used to construct the vapour δD profile.

Author Contribution

SSN carried out all rain and vapour isotopic measurements and part of the data analyses, installed and ran the model BCIM. SPR analyzed most of the samples to get the isotopic data, performed all controlled runs in the BCIM, and constructed most of the figures. SS conceptualized the scientific plan and methodology and wrote the initial draft of the manuscript. SKB contributed to data analysis and interpretation of model outputs, corrected the manuscript, and provided useful comments and suggestions. NA contributed to data analysis and running of the BCIM.

Code Availability

We carried out data analysis and plots using licensed versions of Microsoft Excel and Python, the latter being freely available from https://www.python.org/downloads/. The code of the model, BCIM, is freely available from https://git.app.uib.no/Harald.Sodemann/bcim.

Competing interests

The authors declare that they have no conflict of interest.

Acknowledgements

The Indian Institute of Tropical Meteorology, Pune (IITM), is fully supported by the Earth System Science Organization (ESSO) of the Ministry of Earth Sciences, India. This work forms part of the Ph.D. thesis of SSN, who thanks IITM for a fellowship. SPR thanks IITM for a research associateship. We thank Director IITM for his constant encouragement. The NASA Langley Research Centre and the Atmospheric Science Data Centre are acknowledged for the TES dataset. A fruitful discussion with Dr. Camille Risi is also acknowledged. We thank Dr. Pallab Roy for helping with the Bootstrap analysis and making several plots.

References

Aemisegger, F., Spiegel, J. K., Pfahl, S., Sodemann, H., Eugster, W., and Wernli, H.: Isotope meteorology of cold front passages: A case study combining observations and modeling, Geophys. Res. Lett., 42, 5652–5660, https://doi.org/10.1002/2015GL063988, 2015.

Bacmeister, J. T., Suarez, M. J., and Robertson, F. R.: Rain re-evaporation, boundary layer–convection interactions, and Pacific rainfall patterns in an AGCM, J. Atmos. Sci., 63, 3383–3403, 2006.

Bhattacharya S.K., K. Froehlich, P. K. Aggarwal, and K. M. KulkarniIsotopic variation in Indian Monsoon precipitation: Records from Bombay and New Delhi, Geophysical Research Letters, 30(24), 2285, doi:10.1029/2003GL018453, 2003

Bonne, J. L., Masson-Delmotte, V., Cattani, O., Delmotte, M., Risi, C., Sodemann, H., and Steen-Larsen, H. C.: The isotopic composition of water vapour and precipitation in Ivittuut, southern Greenland, Atmos. Chem. Phys., 14, 4419–4439, https://doi.org/10.5194/acp-14-4419-2014, 2014.

Brubaker, K. L., Entekhabi, D., and Eagleson, P. S.: Estimation of Continental Precipitation Recycling, J. Climate, 6, 1077–1089, https://doi.org/10.1175/1520-0442(1993)006<1077:EOCPR>2.0.CO;2, 1993.

Chakraborty, S., Sinha, N., Chattopadhyay, R., Sengupta, S., Mohan, P. M., and Datye, A.: Atmospheric controls on the precipitation isotopes over the Andaman Islands, Bay of Bengal, Sci. Rep., 6, 19555, https://doi.org/10.1038/srep19555, 2016.

Crawford, J., Hollins, S. E., Meredith, K. T., and Hughes, C. E.: Precipitation stable isotope variability and subcloud evaporation processes in a semi-arid region, Hydrol. Process., 31, 20–34, https://doi.org/10.1002/hyp.10885, 2017.

Dai, Q., Yang, Q., Han, D., Rico-Ramirez, M. A., and Zhang, S.: Adjustment of Radar-Gauge Rainfall Discrepancy Due to Raindrop Drift and Evaporation Using the Weather Research and Forecasting Model and Dual-Polarization Radar, Water Resour. Res., 55, 9211–9233, https://doi.org/10.1029/2019WR025517, 2019.

Dansgaard, W.: Stable isotopes in precipitation, Tellus A: Dynamic Meteorology and Oceanography, 16, 436, https://doi.org/10.3402/tellusa.v16i4.8993, 2012.

Deshpande, R. D., Maurya, A. S., Kumar, B., Sarkar, A., and Gupta, S. K.: Rain-vapor interaction and vapor source identification using stable isotopes from semiarid western India, J. Geophys. Res., 115, 2010JD014458, https://doi.org/10.1029/2010JD014458, 2010.

Draxler, R. R. and Hess, G.: Description of the HYSPLIT4 modeling system, 1997.

Foote, G. B. and du Toit, P. S.: Terminal Velocity of Raindrops Aloft, J. App. Meteorol. (1962-1982), 8, 249–253, 1969.

Farrance, I., and Frenkel, R.: Uncertainty of Measurement: A Review of the Rules for Calculating Uncertainty Components through Functional Relationships, Clin Biochem Rev., 33(2), 49–75, 2012.

Froehlich, K., Kralik, M., Papesch, W., Rank, D., Scheifinger, H., and Stichler, W.: Deuterium excess in precipitation of Alpine regions – moisture recycling, Isotopes in Environmental and Health Studies, 44, 61–70, https://doi.org/10.1080/10256010801887208, 2008.

Gat, J. R.: Oxygen and hydrogen isotopes in the hydrologic cycle, Annu. Rev. Earth Planet. Sci., 24, 225–262, https://doi.org/10.1146/annurev.earth.24.1.225, 1996.

Graf, P., Wernli, H., Pfahl, S., and Sodemann, H.: A new interpretative framework for below-cloud effects on stable water isotopes in vapour and rain, Atmos. Chem. Phys., 19, 747–765, https://doi.org/10.5194/acp-19-747-2019, 2019.

Gray, W. M.: Fundamental Importance of Convective Downdrafts and Mass Recycling Within the Tropical Cloud Cluster and the Typhoon-Hurricane, Trop. Cyclone Res. and Rev., 1, 130–141, https://doi.org/10.6057/2012TCRR01.14, 2012.

Herman, R. L., Cherry, J. E., Young, J., Welker, J. M., Noone, D., Kulawik, S. S., and Worden, J.: Aircraft validation of Aura Tropospheric Emission Spectrometer retrievals of HDO / H_2O, Atmos. Meas. Tech., 7, 3127–3138, https://doi.org/10.5194/amt-7-3127-2014, 2014.

Hersbach, H., Bell, B., Berrisford, P., Hirahara, S., Horányi, A., Muñoz-Sabater, J., Nicolas, J., Peubey, C., Radu, R., Schepers, D., Simmons, A., Soci, C., Abdalla, S., Abellan, X., Balsamo, G., Bechtold, P., Biavati, G., Bidlot, J., Bonavita, M., De Chiara, G., Dahlgren, P., Dee, D., Diamantakis, M., Dragani, R., Flemming, J., Forbes, R., Fuentes, M., Geer, A., Haimberger, L., Healy, S., Hogan, R. J., Hólm, E., Janisková, M., Keeley, S., Laloyaux, P., Lopez, P., Lupu, C., Radnoti, G., De Rosnay, P., Rozum, I., Vamborg, F., Villaume, S., and Thépaut, J.: The ERA5 global reanalysis, Quart. J. Royal Meteorol. Soc., 146, 1999–2049, https://doi.org/10.1002/qj.3803, 2020.

Hwong, Y.L. and Muller, C.J.: The unreasonable efficiency of total rain evaporation removal in triggering convective self-aggregation, Geophys. Res. Lett., *51*, p.e2023GL106523. https://doi.org/10.1029/2023GL106523, 2024.

Ingleby, B., Pauley, P., Kats, A., Ator, J., Keyser, D., Doerenbecher, A., Fucile, E., Hasegawa, J., Toyoda, E., Kleinert, T., Qu, W., St. James, J., Tennant, W., and Weedon, R.: Progress toward high-resolution, real-time radiosonde reports, Bulletin of the American Meteorological Society, 97(11), 2149–2161, https://doi.org/10.1175/BAMS-D-15-00169.1, 2016

IPCC, A.: Climate change 2014 synthesis report, IPCC: Geneva, Switzerland, 1059–1072, 2014.

Jensen, M. P., Holdridge, D. J., Survo, P., Lehtinen, R., Baxter, S., Toto, T., and Johnson, K. L.: Comparison of Vaisala radiosondes RS41 and RS92 at the ARM Southern Great Plains site, Atmos. Meas. Tech., 9, 3115–3129, https://doi.org/10.5194/amt-9-3115-2016, 2016.

Jiang, Y., Yang, L., Li, J., Zeng, Y., Tong, Z., Li, X., and Li, H.: Diurnal variation characteristics of raindrop size distribution observed by a Parsivel2 Disdrometer in the Ili River valley, Adv. in Meteorol. 481661, https://doi.org/10.1155/2024/1481661, 2024.

Konwar, M., Das, S.K., Deshpande, S. M., Chakravarty, K., and Goswami, B. N.: Microphysics of clouds and rain over the Western Ghat, J. Geophys. Res.-Atmos., 119, 6140–6159, https://doi.org/10.1002/2014JD021606, 2014.

Kumar, S., Resmi, E. A., Jash, D., Patade, S., Sumesh, R.K., Andrews, A., Sukumar, N., Aswini, A.R., and Kulkarni, G.: Raindrop size distribution in stratiform precipitation: Insights from spectral bin simulations over the high-altitude cloud physics observatory, Western Ghats. Journal of Atmospheric and Solar-Terrestrial Physics, 277, 106643, 2025

Kumar, S., Hazra, A., and Goswami, B. N.: Role of interaction between dynamics, thermodynamics and cloud microphysics on summer monsoon precipitating clouds over the Myanmar Coast and the Western Ghats, Clim. Dynam., 43, 911–924, https://doi.org/10.1007/s00382-013-1909-3, 2014.

Kumar, T. V. L., Durga, G. P., Rao, K. K., Nagendra, H., and Mall, R. K.: Moisture recycling over the Indian monsoon core region in response to global warming from CMIP5 models, in: Indian Summer Monsoon Variability, Elsevier, 449–466, https://doi.org/10.1016/B978-0-12-822402-1.00008-9, 2021.

Kurita, N.: Water isotopic variability in response to mesoscale convective system over the tropical ocean, J. Geophys. Res.-Atmos., 118, https://doi.org/10.1002/jgrd.50754, 2013.

Law, S.L.G., Kuok, K. K., and Trinidad, S.G.: An Experimental Study on The Correlation of Natural Rainfall Intensities and Raindrop Size Distribution Characteristics, 2021 IOP Conf. Ser.: Mater. Sci. Eng. 1101 012009, 10.1088/1757-899X/1101/1/012009, 2021

Lee, C., Lawson, W. G., Richardson, M. I., Anderson, J. L., Collins, N., Hoar, T., and Mischna, M.: Demonstration of ensemble data assimilation for Mars using DART, MarsWRF, and radiance observations from MGS TES, J. Geophys. Res., 116, E11011, https://doi.org/10.1029/2011JE003815, 2011.

Lee, J. and Fung, I.: Amount effect of water isotopes and quantitative analysis of post-condensation processes, Hydrol. Process., 22, 1–8, https://doi.org/10.1002/hyp.6637, 2008.

Lekshmy, P. R., Midhun, M., Ramesh, R., and Jani, R. A.: ^{18}O depletion in monsoon rain relates to large-scale organized convection rather than the amount of rainfall, Sci. Rep., 4, 5661, https://doi.org/10.1038/srep05661, 2014.

Lekshmy, P. R., Midhun, M., and Ramesh, R.: Influence of stratiform clouds on δD and $\delta^{18}O$ of monsoon water vapour and rain at two tropical coastal stations, J. Hydrol., 563, 354–362, https://doi.org/10.1016/j.jhydrol.2018.06.001, 2018.

Levine, R. C. and Turner, A. G.: Dependence of Indian monsoon rainfall on moisture fluxes across the Arabian Sea and the impact of coupled model sea surface temperature biases, Clim. Dynam., 38, 2167–2190, https://doi.org/10.1007/s00382-011-1096-z, 2012.

Li, X. and Srivastava, R. C.: An Analytical Solution for Raindrop Evaporation and Its Application to Radar Rainfall Measurements, J. Appl. Meteorol., 40, 1607–1616, https://doi.org/10.1175/1520-0450(2001)040<1607:AASFRE>2.0.CO;2, 2001.

Li, X., Tang, C., and Cui, J.: Intra-Event Isotopic Changes in Water Vapor and Precipitation in South China, Water, 13, 940, https://doi.org/10.3390/w13070940, 2021.

Marshall, J. S., and Palmer, W. mcK.: The distribution of raindrops with size, Journal of Meteorology, Shorter contributions, 5, 165-166, 1948

Mandke, S.K., Soman, M. K., and Satyan, V.: Impact of Convective Downdrafts in a GCM on the Simulated Mean Indian Summer Monsoon and its Variability, J. Meteorol. Soc. Jpn, 77, 1061–1082, https://doi.org/10.2151/jmsj1965.77.5_1061, 1999.

Midhun, M., Lekshmy, P. R., Ramesh, R., Yoshimura, K., Sandeep, K. K., Kumar, S., Sinha, R., Singh, A., and Srivastava, S.: The Effect of Monsoon Circulation on the Stable Isotopic Composition of Rainfall, J. Geophys. Res.-Atmos., 123, 5205–5221, https://doi.org/10.1029/2017JD027427, 2018.

Moerman, J. W., Cobb, K. M., Adkins, J. F., Sodemann, H., Clark, B., and Tuen, A. A.: Diurnal to interannual rainfall $\delta^{18}O$ variations in northern Borneo driven by regional hydrology, Earth Planet. Sci. Lett., 369–370, 108–119, https://doi.org/10.1016/j.epsl.2013.03.014, 2013.

Morrison, H., van Lier-Walqui, M., Fridlind, A. M., Grabowski, W. W.,Harrington, J. Y., Hoose, C., et al.: Confronting the challenge ofmodeling cloud and precipitationmicrophysics. Journal of Advances inModeling Earth Systems, 12, e2019MS001689. https://doi.org/10.1029/2019MS001689, 2020.

Munksgaard, N. C., Zwart, C., Haig, J., Cernusak, L. A., and Bird, M. I.: Coupled rainfall and water vapour stable isotope time series reveal tropical atmospheric processes on multiple timescales, Hydrol. Process., 34, 111–124, https://doi.org/10.1002/hyp.13576, 2020.

Murali Krishna, U. V., Das, S. K., Sulochana, E. G., Bhowmik, U., Deshpande, S. M., and Pandithurai, G.: Statistical characteristics of raindrop size distribution over the Western Ghats of India: wet versus dry spells of the Indian summer monsoon, Atmos. Chem. Phys., 21, 4741–4757, https://doi.org/10.5194/acp-21-4741-2021, 2021.

Naik, M,, Jadhav, A. V., Mukhim, S., Kumar, P. P., and Rohini, L.: Bhawar-Cloud base height variability observed using a Laser- Based Ceilometer over a tropical station Pune, India International Journal of Remote Sensing, 45, https://doi.org/10.1080/01431161.2024.2402003, 2003.

Nimya, S. S., Sengupta, S., Parekh, A., Bhattacharya, S. K., and Pradhan, R.: Region-specific performances of isotope enabled general circulation models for Indian summer monsoon and the factors controlling isotope biases, Clim. Dynam., 59, 3599–3619, https://doi.org/10.1007/s00382-022-06286-1, 2022.

Noone D.: Pairing Measurements of the Water Vapor Isotope Ratio with Humidity to Deduce Atmospheric Moistening and Dehydration in the Tropical Mid-troposphere, Journal of climate, 25(13), 4476-4494, https://doi.org/10.1175/JCLI-D-11-00582.1, 2012.

Padmakumari, B., Maheskumar, R. S., Morwal, S.B., and Kulkarni, J. R.: Variability of Index of Coalescence Activity (ICA) over a rain-shadow region during monsoon and its role in cloud seeding programs in India, Atmospheric Research, 304, 107390, 2024

Pathak, A., Ghosh, S., and Kumar, P.: Precipitation Recycling in the Indian Subcontinent during Summer Monsoon, J. Hydrometeorol., 15, 2050–2066, https://doi.org/10.1175/JHM-D-13-0172.1, 2014.

Pattanaik, D., Mandal, R., Dey, A., Phani, R., Chattopadhyay, R., Joseph, S., Sahai, A., and Mohapatra, M.: Extended Range Forecast (ERF) During Southwest Monsoon 2019, 2019.

Pfahl, S., Wernli, H., and Yoshimura, K.: The isotopic composition of precipitation from a winter storm – A case study with the limited-area model $COSMO_{iso}$, Atmos. Chem. Phys., 12, 1629–1648, https://doi.org/10.5194/acp-12-1629-2012, 2012.

Pradhan, R., Singh, N., and Singh, R. P.: Onset of summer monsoon in Northeast India is preceded by enhanced transpiration, Sci. Rep., 9, 18646, https://doi.org/10.1038/s41598-019-55186-8, 2019.

Pranindita, A., Wang-Erlandsson, L., Fetzer, I., and Teuling, A. J.: Moisture recycling and the potential role of forests as moisture source during European heatwaves, Clim. Dynam., 58, 609–624, https://doi.org/10.1007/s00382-021-05921-7, 2022.

Pruppacher, H. R., and Klett, J. D.: Microstructure of Atmospheric Clouds and Precipitation, in: Microphysics of Clouds and Precipitation, vol. 18, Springer Netherlands, Dordrecht, 10–73, https://doi.org/10.1007/978-0-306-48100-0_2, 2010.

Rahul, P., Ghosh, P., Bhattacharya, S.K., and Yoshimura, K.: Controlling factors of rainwater and water vapor isotopes at Bangalore, India: Constraints from observations in 2013 Indian monsoon, J. Geophys. Res.-Atmos., 121, https://doi.org/10.1002/2016JD025352, 2016.

Rajaveni, S. P., Nimya, S. S., Sengupta, S., Datye, A., and Sarma, D.: Three Years of Stable Water Isotope Data of Daily Rain Samples Collected from Three Geomorphic Regions of India, Sci. Data, 11, 1445, https://doi.org/10.1038/s41597-024-04308-7, 2024.

Rao, Y.P.: Southwest Monsoon, Meteorological Monograph Synoptic Meteorology No.1., India Meteorological Department, 1976.

Risi, C., Bony, S., and Vimeux, F.: Influence of convective processes on the isotopic composition (δ^{18}O and δD) of precipitation and water vapor in the tropics: 2. Physical interpretation of the amount effect, J. Geophys. Res., 113, 2008JD009943, https://doi.org/10.1029/2008JD009943, 2008.

Risi, C., Bony, S., Vimeux, F., and Jouzel, J.: Water-stable isotopes in the LMDZ4 general circulation model: Model evaluation for present-day and past climates and applications to climatic interpretations of tropical isotopic records, J. Geophys. Res.-Atmos., 115, https://doi.org/10.1029/2009JD013255, 2010.

Risi, C., Galewsky, J., Reverdin, G., and Brient, F.: Controls on the water vapor isotopic composition near the surface of tropical oceans and role of boundary layer mixing processes, Atmos. Chem. Phys., 19, 12235–12260, https://doi.org/10.5194/acp-19-12235-2019, 2019.

Risi, C., Muller, C., and Blossey, P.: Rain Evaporation, Snow Melt, and Entrainment at the Heart of Water Vapor Isotopic Variations in the Tropical Troposphere, According to Large-Eddy Simulations and a Two-Column Model, J. Adv. Model Earth Syst., 13, e2020MS002381, https://doi.org/10.1029/2020MS002381, 2021.

Risi, C., Muller, C., Vimeux, F., Blossey, P., Védeau, G., Dufaux, C., and Abramian, S.: What Controls the Mesoscale Variations in Water Isotopic Composition Within Tropical Cyclones and Squall Lines? Cloud

Resolving Model Simulations in Radiative-Convective Equilibrium, J. Adv. Model Earth Syst., 15, e2022MS003331, https://doi.org/10.1029/2022MS003331, 2023.

Ryu, S., Song, J. J., and Lee, G. W.: Radar–Rain Gauge Merging for High-Spatiotemporal-Resolution Rainfall Estimation Using Radial Basis Function Interpolation, Remote Sens. 17(3), 530; https://doi.org/10.3390/rs17030530, 2025

Salamalikis, V., Argiriou, A. A., and Dotsika, E.: Isotopic modeling of the sub-cloud evaporation effect in precipitation, Sci. Total Environ., 544, 1059–1072, https://doi.org/10.1016/j.scitotenv.2015.11.072, 2016.

Sapucci, L. F., Machado, L. A. T., Da Silveira, R. B., Fisch, G., Monico, J. F. G.: Analysis of Relative Humidity Sensors at the WMO Radiosonde Intercomparison Experiment in Brazil, Journal of Atmospheric And Oceanic Technology, 22, 664-678, 2005.

Saranya, P., Krishan, G., Rao, M. S., Kumar, S., and Kumar, B.: Controls on water vapor isotopes over Roorkee, India: Impact of convective activities and depression systems, J. Hydrol., 557, 679–687, https://doi.org/10.1016/j.jhydrol.2017.12.061, 2018.

Sarkar, M., Bailey, A., Blossey, P., de Szoeke, S. P., Noone, D., Quiñones Meléndez, E., Leandro, M. D., and Chuang, P. Y.: Sub-cloud rain evaporation in the North Atlantic winter trade winds derived by pairing isotopic data with a bin-resolved microphysical model, Atmos. Chem. Phys., 23, 12671–12690, https://doi.org/10.5194/acp-23-12671-2023, 2023.

Sengupta, S., Bhattacharya, S. K., Parekh, A., Nimya, S. S., Yoshimura, K., and Sarkar, A.: Signatures of monsoon intra-seasonal oscillation and stratiform process in rain isotope variability in northern Bay of Bengal and their simulation by isotope enabled general circulation model, Clim. Dynam., 55, 1649–1663, https://doi.org/10.1007/s00382-020-05344-w, 2020.

Sengupta, S., Bhattacharya, S. K., Sunil, N. S., and Sonar, S.: Quantifying Raindrop Evaporation Deficit in General Circulation Models from Observed and Model Rain Isotope Ratios on the West Coast of India, Atmosphere, 14, 1147, https://doi.org/10.3390/atmos14071147, 2023.

Sinha, N. and Chakraborty, S.: Isotopic interaction and source moisture control on the isotopic composition of rainfall over the Bay of Bengal, Atmos. Res., 235, 104760, https://doi.org/10.1016/j.atmosres.2019.104760, 2020.

Sodemann, H., Aemisegger, F., Pfahl, S., Bitter, M., Corsmeier, U., Feuerle, T., Graf, P., Hankers, R., Hsiao, G., Schulz, H., Wieser, A., and Wernli, H.: The stable isotopic composition of water vapour above Corsica during the HyMeX SOP1 campaign: insight into vertical mixing processes from lower-tropospheric survey flights, Atmos. Chem. Phys., 17, 6125–6151, https://doi.org/10.5194/acp-17-6125-2017, 2017.

Stewart, M. K.: Stable isotope fractionation due to evaporation and isotopic exchange of falling waterdrops: Applications to atmospheric processes and evaporation of lakes, J. Geophys. Res., 80, 1133–1146, https://doi.org/10.1029/JC080i009p01133, 1975.

Tao, W., Chen, J., Li, Z., Wang, C., and Zhang, C.: Impact of aerosols on convective clouds and precipitation, Rev. Geophys., 50, 2011RG000369, https://doi.org/10.1029/2011RG000369, 2012.

Trenberth, K. E.: Atmospheric Moisture Recycling: Role of Advection and Local Evaporation, J. Climate, 12, 1368–1381, https://doi.org/10.1175/1520-0442(1999)012<1368:AMRROA>2.0.CO;2, 1999.

Utsav, B., Deshpande, S. M., Das, S. K., and Pandithurai, G.: Statistical Characteristics of Convective Clouds over the Western Ghats Derived from Weather Radar Observations, J. Geophys. Res.-Atmos., 122, https://doi.org/10.1002/2016JD026183, 2017.

Villiger, L., Dütsch, M., Bony, S., Lothon, M., Pfahl, S., Wernli, H., Brilouet, P.-E., Chazette, P., Coutris, P., Delanoë, J., Flamant, C., Schwarzenboeck, A., Werner, M., and Aemisegger, F.: Water isotopic characterisation of the cloud–circulation coupling in the North Atlantic trades – Part 1: A process-oriented evaluation of COSMOiso simulations with EUREC4A observations, Atmos. Chem. Phys., 23, 14643–14672,

https://doi.org/10.5194/acp-23-14643-2023, 2023.

Vimeux, F., Tremoy, G., Risi, C., and Gallaire, R.: A strong control of the South American SeeSaw on the intra-seasonal variability of the isotopic composition of precipitation in the Bolivian Andes, Earth and Planet. Sci. Lett., 307, 47–58, https://doi.org/10.1016/j.epsl.2011.04.031, 2011.

Wang, B., Ding, Y., and Sikka, D.: Synoptic systems and weather, The Asian Monsoon, 131–201, 2006.

Wang, R., Gentine, P., Yin, J., Chen, L., Chen, J., and Li, L.: Long-term relative decline in evapotranspiration with increasing runoff on fractional land surfaces, Hydrol. Earth Syst. Sci., 25, 3805–3818, https://doi.org/10.5194/hess-25-3805-2021, 2021.

Wang, S., Zhang, M., Che, Y., Chen, F., and Qiang, F.: Contribution of recycled moisture to precipitation in oases of arid central Asia: A stable isotope approach, Water Resour. Res., 52, 3246–3257, https://doi.org/10.1002/2015WR018135, 2016.

Worden, J., Noone, D., Bowman, K. et al.: Importance of rain evaporation and continental convection in the tropical water cycle, Nature, 445, 528–532, https://doi.org/10.1038/nature05508, 2007.

Worden, J., Noone, D., Galewsky, J., Bailey, A., Bowman, K., Brown, D., Hurley, J., Kulawik, S., Lee, J., and Strong, M.: Estimate of bias in Aura TES HDO/H_2O profiles from comparison of TES and in situ HDO/H_2O measurements at the Mauna Loa observatory, Atmos. Chem. Phys., 11, 4491–4503, https://doi.org/10.5194/acp-11-4491-2011, 2011.

Wu, Y., Gao, J., Zhao, A., Niu, X., Liu, Y., Ratnasekera, D., Gamage, T. P., and Samantha, A. H. R.: One-year continuous observations of near-surface atmospheric water vapor stable isotopes at Matara, Sri Lanka, reveal a strong link to moisture sources and convective intensity, Atmos. Chem. Phys., 25, 4013–4033, https://doi.org/10.5194/acp-25-4013-2025, 2025.

Xiao, F., Zhu, B., and Zhu, T.: Inconsistent urbanisation effects on summer precipitation over the typical climate regions in central and eastern China, Theor. Appl. Climatol., 143, 73–85, https://doi.org/10.1007/s00704-020-03404-z, 2021.

Xie, X., Evaristo, R., Troemel, S., Saavedra, P., Simmer, C., and Ryzhkov, A.: Radar Observation of Evaporation and Implications for Quantitative Precipitation and Cooling Rate Estimation, J. Atmos. and Ocean. Technol., 33, 1779–1792, https://doi.org/10.1175/JTECH-D-15-0244.1, 2016.

Xing, M., Liu, W., and Hu, J.: A set of methods to quantitatively evaluate the below-cloud evaporation effect on precipitation isotopic composition: a case study in a city located in the semi-arid regions of Chinese Loess Plateau, https://doi.org/10.5194/acp-2020-312, 26 May 2020.

Xu, H., Guo, J., Tong, B., Zhang, J., Chen, T., Guo, X., Zhang, J., and Chen, W.: Characterizing the near-global cloud vertical structures over land using high-resolution radiosonde measurements, Atmos. Chem. Phys., 23, 15011–15038, https://doi.org/10.5194/acp-23-15011-2023, 2023.

Yoshimura, K., Kanamitsu, M., Noone, D., and Oki, T.: Historical isotope simulation using Reanalysis atmospheric data, J. Geophys. Res., 113, 2008JD010074, https://doi.org/10.1029/2008JD010074, 2008.

Zaitchik, B. F., Macalady, A. K., Bonneau, L. R., and Smith, R. B.: Europe's 2003 heat wave: a satellite view of impacts and land–atmosphere feedbacks, Int. J. Climatol., 26, 743–769, https://doi.org/10.1002/joc.1280, 2006.

Zhang, F., Huang, T., Man, W., Hu, H., Long, Y., Li, Z., and Pang, Z.: Contribution of Recycled Moisture to Precipitation: A Modified d-Excess-Based Model, Geophys. Res. Lett., 48, e2021GL095909, https://doi.org/10.1029/2021GL095909, 2021.

Zhu, G., Zhang, Z., Guo, H., Zhang, Y., Yong, L., Wan, Q., Sun, Z., and Ma, H.: Below-Cloud Evaporation of Precipitation Isotopes over Mountains, Oases, and Deserts in Arid Areas, J. Hydrometeorol., 22, 2533–2545, https://doi.org/10.1175/JHM-D-20-0170.1, 2021.